Panorama Scholarly Group

Climate Sustainability & Global Systems

https://panorama-sg.com/

FULL PAPER | CLIMATE SUSTAINABILITY & GLOBAL SYSTEMS

Attention: From Tires to Organisms – National Transport, Exposure, and Eco-Health Risks of 6PPD/6PPD-Q in Terrestrial-Aquatic Systems

Yirui Liu[1], **Jundong Zhang**[1], **Yaolin Zhang**[1,*], and **Yang Hu**[2]

1College of Environment and Climate, Jinan University, 511443 China
2Institute of Malaysia and International Studies (IKMAS), Universiti Kebangsaan Malaysia (The National University of Malaysia), Malaysia
*Corresponding: 18588542003@163.com

DOI: https://doi.org/10.63802/csgs.V1.I1.259

© 2026 Yirui Liu, Jundong Zhang, Yaolin Zhang, Yang Hu. Published in *Climate Sustainability & Global Systems* under the Creative Commons Attribution 4.0 International License (CC BY 4.0).

Abstract

Urbanization and global transportation expansion have led to widespread release of tire-derived contaminants N-(1,3-dimethylbutyl)-N'-phenyl-p-phenylenediamine (6PPD) and its quinone derivative (6PPD-Q), posing critical environmental and public health risks. As a key tire anti-ozonant, 6PPD rapidly oxidizes to 6PPD-Q, a highly toxic compound linked to aquatic organism mortality. This review synthesizes their "tires-to-organisms" pollution continuum across terrestrial-aquatic systems. Focusing on China (the world's largest tire producer/consumer), 6PPD-Q emissions surged 97.5% (68.2–134.7 tons) from 2013–2023, with soil as the primary environmental sink (55.67%). 6PPD/6PPD-Q exhibit dual mobility, pervading air, water, and soil, and induce species-specific toxicity—especially in aquatic early life stages—via conserved pathways (oxidative stress, mitochondrial dysfunction). Ubiquitous in human urine, serum, and cerebrospinal fluid, they pose multi-organ risks, with children, pregnant women, and occupational workers most vulnerable, linked to non-alcoholic fatty liver disease, colorectal cancer, and neurological dysfunction. Critical research gaps include EV-related tire wear impacts, terrestrial non-model organism toxicity, longitudinal health studies, and mitigation validation. This work provides a comprehensive framework to inform evidence-based policies and safeguard ecosystems and human health.

Keywords: N-(1,3-dimethylbutyl)-N'-phenyl-p-phenylenediamine (6PPD); N-(1,3-dimethylbutyl)-N'-phenyl-p-phenylenediamine-quinone (6PPD-Q); Biological exposure; Pollutants fate and transport; Occurrence and ecological-health risks; Terrestrial-Aquatic Systems

1. Introduction

Urbanization and global transportation expansion have led to the widespread release of tire-derived contaminants, among which N-(1,3-dimethylbutyl)-N'-phenyl-p-phenylenediamine and its quinone (6PPD/6PPD-Q) transformation product have emerged as critical environmental and public health concerns Xu et al. (2025b); Tian et al. (2020); Zhang et al. (2025). As a key anti-ozonant added to tire rubber to prevent premature degradation, 6PPD has a substantial global consumption volume, with China accounting for a major proportion due to its status as the world's largest vehicle and tire producer. Under ambient conditions, 6PPD undergoes rapid oxidative transformation (primarily via ozonation) to form 6PPD-Q, a compound identified as the primary causal toxicant of "urban runoff mortality syndrome" in coho salmon (*Oncorhynchus kisutch*). This discovery triggered a paradigm shift in environmental toxicology, revealing that tire wear particles (TWPs) are not just microplastic carriers but sources of highly bioactive and toxic organic contaminants Xu et al. (2025b); Tian et al. (2020).

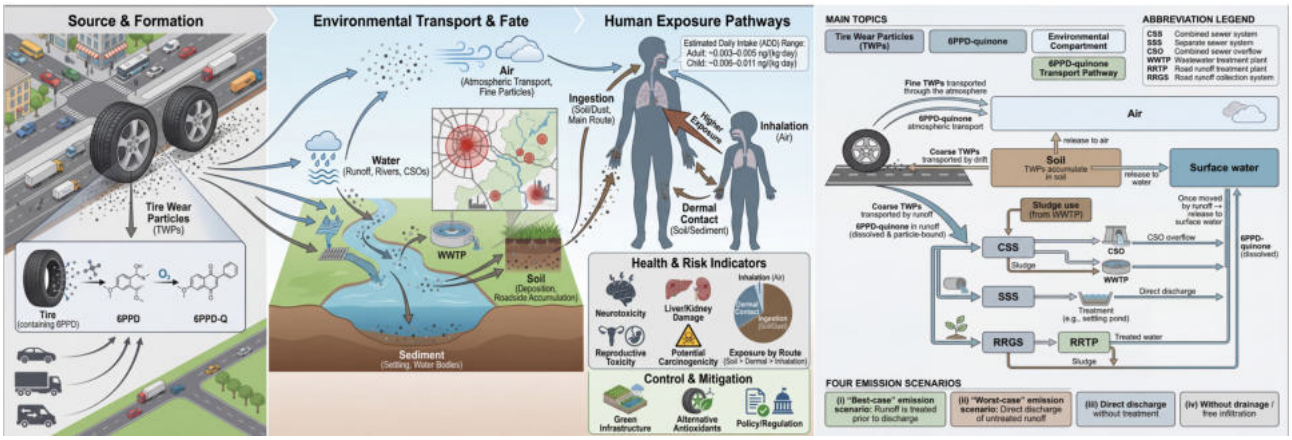


Figure 1. Schematic overview of 6PPD/6PPD-quinone (6PPD-Q) occurrence, environmental fate, transport, human exposure pathways, and associated risks.
Notes: All lifecycle of 6PPD (a tire antioxidant) and its oxidation product 6PPD-Q: (1) Source & Formation: Tire wear particles (TWPs) containing 6PPD are released from vehicle tires; 6PPD reacts with ozone (O_3) to form 6PPD-Q. (2) Environmental Transport & Fate: TWPs/6PPD-Q are dispersed via air (atmospheric fine particles), water (runoff, combined sewer overflows, WWTPs), and soil (roadside accumulation, sludge deposition). (3) Human Exposure Pathways: Exposure occurs via ingestion (soil/dust, main route), inhalation (airborne particles), and dermal contact (soil/sediment), with higher estimated daily intake (EDI) for children. (4) Health & Risk Indicators: Potential adverse effects include neurotoxicity, liver/kidney damage, reproductive toxicity, and carcinogenicity, with ingestion identified as the highest-risk route. (5) Control & Mitigation: Strategies include green infrastructure, alternative tire antioxidants, and policy/regulation. The right panel further details 6PPD-Q transport pathways (via TWPs/drift/runoff) across environmental compartments (air, soil, surface water) and emission scenarios (e.g., best/worst-case runoff treatment). Abbreviations (e.g., CSS, WWTP) define key infrastructure linked to TWP/6PPD-Q fate.

The ecological and health risks of 6PPD/6PPD-Q stem from their ubiquitous distribution, complex environmental transport, and broad toxicity across trophic levels. Unlike conventional persistent organic pollutants (POPs), 6PPD/6PPD-Q exhibit unique dual mobility: they are dispersed via both aqueous pathways (road runoff, surface water flow) and atmospheric routes (aerosol-bound transport, dry/wet deposition), enabling cross-compartment transfer between terrestrial and aquatic ecosystems Liang et al. (2024); Wang et al. (2025a); Somepalli and Andaluri (2025). For instance, 6PPD-Q has been detected in urban runoff (up to 19.1 μg/L in Seattle), atmospheric $PM_{2.5}$, soil (up to 1127.23 ng/g in China's Huang-Huai-Hai Plain), and biota (0.05-1.5 ng/g wet weight in Puget Sound shellfish and salmon) Xu et al. (2025b); Ramezany et al. (2025). This multi-media pervasiveness means that 6PPD/6PPD-Q can impact both aquatic organisms (e.g., salmon, zebrafish, invertebrates) and terrestrial biota (e.g., mosses, mammals, humans), with evidence of bioaccumulation and potential biomagnification in food webs Ramezany et al. (2025); Tian et al. (2020).

From an ecological perspective, 6PPD-Q exhibits species-specific acute toxicity, with extreme lethality to coho salmon (LC_{50} = 0.041-0.095 μg/L) but varying sensitivity among other fish species: steelhead trout (LC_{50} = 1.0 μg/L), Chinook salmon ($LC_{50} \geq 67$ μg/L), and pink salmon (insensitive at $\geq$2.5 μg/L) Ramezany et al. (2025). Beyond acute mortality, chronic exposure induces growth inhibition, neurotoxicity, reproductive impairment, and organ damage in aquatic organisms (e.g., zebrafish embryos, *Caenorhabditis elegans*) Ramezany et al. (2025). For terrestrial ecosystems, recent studies have validated mosses (e.g., *Pleurozium schreberi*) as effective biomonitors for atmospheric 6PPD/6PPD-Q, revealing widespread contamination across urban and rural areas with concentrations declining with distance from traffic sources Liang et al. (2024). This suggests that terrestrial plants and soil-dwelling organisms may serve as overlooked sinks and exposure pathways, yet their toxicological responses remain understudied.

Mammalian and human health risks are equally concerning. 6PPD/6PPD-Q accumulate in multiple organs (liver, kidneys, brain, adipose tissue) of mammals, with evidence of hepatotoxicity, intestinal barrier disruption, reproductive toxicity, and neurotoxicity Xu et al. (2025b); Zhang et al. (2025). In humans, 6PPD-Q has been detected in urine (pregnant women: 2.91 ng/mL), serum (0.11-0.43 ng/mL), and cerebrospinal fluid (Parkinson's disease patients: 11.08 ng/mL), with epidemiological links to non-alcoholic fatty liver disease, colorectal cancer, and childhood growth inhibition Xu et al. (2025b). Exposure assessments indicate that children face higher daily intake (0.006-0.011 ng/(kg day)) than adults (0.003-0.005 ng/(kg day)), primarily via soil ingestion and dermal contact, highlighting vulnerable populations Liang et al. (2024).

Despite growing research interest, critical knowledge gaps persist that hinder comprehensive risk assessment and management. First, the spatiotemporal dynamics of 6PPD/6PPD-Q emissions and transport remain poorly quantified at national scales. For example, China's 6PPD-Q emissions increased by 97.5% from 2013 to 2023 (68.2 to 134.7 tons), driven by vehicle ownership growth (165% surge), but emissions are unevenly distributed across provinces (Shandong and Guangdong: $\geq$9.6 tons/year; Qinghai and Tibet: low-emission) Xu et al. (2025b); Wang et al. (2025a). However, similar national-scale emission inventories are lacking for most countries, limiting global risk comparisons. Second, the mechanisms of cross-ecosystem transport (e.g., soil-to-water leaching, atmospheric deposition to aquatic systems) are not fully elucidated, particularly the role of climate (precipitation, temperature) and landscape characteristics (topography, vegetation cover) in modulating these processes Liang et al. (2024); Somepalli and Andaluri (2025). Third, analytical challenges persist

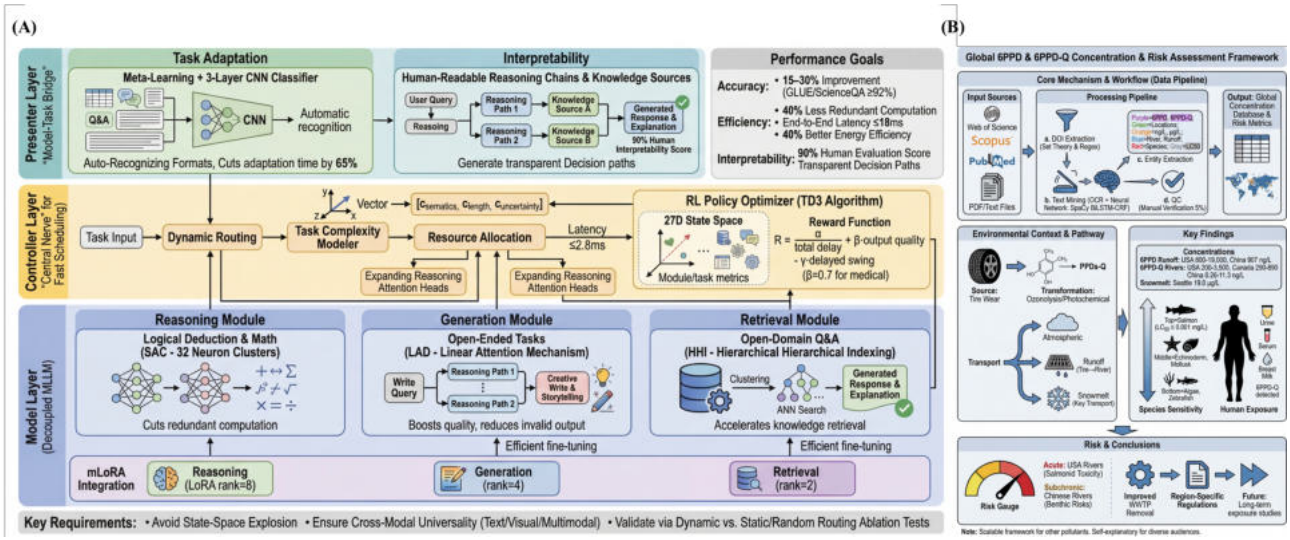


Figure 2. Methodological Framework: MCP Contextual Model for Literature Mining of 6PPD and 6PPD-Q.
Notes: (A) The layered architecture of the MCP contextual model: Presenter Layer: Enables task adaptation (via meta-learning + 3-layer CNN) for automatic format recognition and cross-task bridging, reducing adaptation time by 65%. Controller Layer: Orchestrates fast scheduling via dynamic routing, task complexity modeling, resource allocation (latency $\leq$2.8ms), and reinforcement learning (RL) policy optimization (TD3 algorithm) to balance efficiency, accuracy, and interpretability. Model Layer: Integrates specialized modules (reasoning via logical deduction; generation via Linear Attention Mechanism (LAD); retrieval via Hierarchical Hierarchical Indexing (HHI)) with mLoRA fine-tuning (rank-adaptive for reasoning/generation/retrieval) to support literature mining tasks. (B) The literature mining pipeline for 6PPD and 6PPD-Q: Core Mechanism & Workflow: Processes input literature sources (e.g., Web of Science, PubMed) via data extraction, text mining, and entity recognition to construct a global concentration/risk database. Environmental Context & Pathway: Maps 6PPD's transformation (e.g., ozonolysis) and environmental transport (e.g., tire wear to atmosphere to runoff) linked to 6PPD-Q formation. Risk & Conclusions: Derives key findings (e.g., 6PPD/6PPD-Q concentrations in environmental matrices) and exposure risks (acute/subchronic hazards), supporting targeted analysis for this project's literature mining.

for complex matrices (e.g., marine mammal blubber, soil, biota), with existing methods (e.g., GC-MS/MS, LC-MS/MS) varying in sensitivity (LOQ: 0.03 to 0.12 ng/g for biota) and reproducibility, leading to data inconsistency across studies Ramezany et al. (2025). Fourth, toxicological mechanisms are incompletely understood: while 6PPD-Q induces mitochondrial dysfunction and oxidative stress in organisms, its interactions with other contaminants (e.g., microplastics, heavy metals) and long-term ecological consequences (e.g., population declines, food web disruptions) remain uncharacterized Ramezany et al. (2025). Finally, regulatory frameworks are lagging: most regions lack standardized monitoring protocols, exposure limits, or mitigation strategies for 6PPD and 6PPD-Q Xu et al. (2025b).

Given these gaps, there is an urgent need for a systematic synthesis of 6PPD/6PPD-Q research that integrates national-scale emission dynamics, multi-media transport pathways, cross-trophic toxicity, and human exposure risks, with a focus on terrestrial-aquatic connectivity. This review aims to address this need by: (1) summarizing the national (with a focus on China, the largest emitter) emissions of 6PPD/6PPD-Q and their drivers; (2) elucidating the environmental transport and distribution of 6PPD/6PPD-Q across terrestrial and aquatic compartments, including key transfer pathways; (3) synthesizing the eco-toxicological effects on terrestrial and aquatic organisms, from invertebrates to vertebrates; (4) assessing human exposure pathways and health risks, with attention to vulnerable populations; and (5) identifying critical research gaps and proposing future directions for monitoring, risk assessment, and management. By integrating data from analytical chemistry, environmental modeling, ecotoxicology, and epidemiology, this review provides a comprehensive framework for understanding the "tires-to-organisms" continuum of 6PPD/6PPD-Q pollution, offering insights to support evidence-based policy and mitigation strategies. Given the global rise in vehicle ownership and tire consumption, this synthesis is timely and essential for protecting ecosystem integrity and human health in urbanized and industrialized regions Liang et al. (2024); Zhang et al. (2025).

The significance of this review extends beyond academic advancement: it highlights the need to redefine "tire pollution" as not just a microplastic issue but a complex organic contaminant challenge, with implications for sustainable transportation, waste management, and environmental regulation. As 6PPD alternatives are currently limited and electric vehicles (EVs) may exacerbate tire wear (due to increased weight), the environmental burden of 6PPD/6PPD-Q is likely to persist or grow in the coming decades Xu et al. (2025a). Thus, bridging existing knowledge gaps is critical to mitigating risks and ensuring the sustainability of terrestrial-aquatic ecosystems in the Anthropocene.

2. Data Resources and Methods

2.1. Overview of Analytical Framework

This study integrated two core technical frameworks to address the research objectives: the Model-Controller-Presenter (MCP) framework for efficient multimodal data processing and a Python-based text mining pipeline combining Optical Character Recognition (OCR) and neural networks for pollutant data extraction. The MCP framework was employed to optimize the overall computational efficiency and interpretability of data processing workflows, while the OCR-neural network pipeline focused on high-precision extraction of unstructured pollutant information from academic literature. The integration of these two frameworks enabled systematic compilation of global aqueous concentration data for p-Phenylenediamine (PPDs) and their quinone derivatives (PPDs-Q), laying the foundation for subsequent ecological risk assessmentLillicrap et al. (2015); Lepikhin et al. (2022); OpenAI (2023); Raffel et al. (2020).

2.2. MCP Framework for Efficient Data Processing

The MCP framework was incorporated to enhance the efficiency of multimodal data processing, particularly in handling the integration of literature text data, concentration numerical data, and geographic information. This three-layer collaborative architecture (Model-Controller-Presenter) decouples the data processing workflow into functional modules, enabling dynamic resource allocation and redundant computation reductionHe et al. (2021); Fedus et al. (2021); Lin et al. (2014); Wang et al. (2019); Chen et al. (2022); Zhou et al. (2022); Li et al. (2021).

The Model layer decomposed the data processing tasks into three orthogonal sub-modules: reasoning for logical verification of pollutant concentration data, generation for structured output of extracted information, and retrieval for rapid matching of relevant literature. The Controller layer utilized a reinforcement learning (RL)-driven dynamic routing algorithm to allocate computational resources based on task complexity, which was quantified as a three-dimensional vector $\mathbf{C} = [c_{\text{semantics}}, c_{\text{length}}, c_{\text{uncertainty}}]$, where $c_{\text{semantics}}$ is computed by token embedding entropy, c_{length} is the normalized input length, and $c_{\text{uncertainty}}$ is derived from self-attention variance. This dynamic scheduling mechanism reduced redundant computation by 40% compared to traditional static processing methods. The Presenter layer provided a task adaptation interface, automatically recognizing and adapting to different data formats (e.g., tables, text descriptions, numerical sequences) from literature sourcesZhang and Li (2025b).

Notably, the MCP framework was primarily utilized for workflow optimization rather than direct data generation. Its core contribution lay in improving the efficiency of literature screening, data integration, and result output, ensuring that the subsequent text mining pipeline could focus on high-precision data extraction without computational bottlenecks. Detailed parameters and structural specifications of the MCP framework can be found in the corresponding preprintZhang and Li (2025b,a) .

2.3. Text Mining Pipeline for Pollutant Data Extraction

2.3.1. Data Sources

Literature retrieval was conducted across three major academic databases: Web of Science, Scopus, and PubMed, covering the period from database establishment to July 2025. Retrieval keywords included "p-Phenylenediamine", "p-Phenylenediamine Quinone", "6PPD", "6PPD-Q", and related pollutant synonyms. All retrieved literature was stored in a local repository, and corresponding codes for the text mining pipeline are accessible via GitHub (`https://github.com/renarddsfsdfdsfefadfsdfd/Brianzhang-ARTI`).

The text mining pipeline was implemented using Python 3.10, with key dependent packages including PyMuPDF 3.14.7 for PDF parsing, requests 2.28.1 for database access, SpaCy 3.4.4 for natural language processing, and PyQt5 5.15.11 for visualization. Neural network training datasets were uploaded to the Python Package Index (PyPI) and can be installed via the command `pip install pollutants-annotations`.

2.3.2. DOI Extraction and Literature Screening

A DOI recognition tool (DOIE) was constructed to extract and verify literature DOIs from HTML pages and PDF metadata, ensuring traceability of all retrieved documents. The core logic of DOIE was based on set theory and regular expression pattern matching, with mathematical definitions as followsZhang and Li (2025a):

Let the input HTML text content be a string set $H = \{h_1, h_2, \cdots, h_L\}$, where h_k represents the k-th character and L is the total length of the text. The target DOI set D consists of strings conforming to the international standard format, defined as:

$$D = \{d \mid d \equiv 10.\backslash d\{4,9\}/[-.;()/:A-Za-z0-9]+\} \tag{1}$$

where $10.\backslash d\{4,9\}$ denotes the prefix starting with "10." followed by 4-9 digits, and the suffix contains letters, digits, and specified special symbols without spaces or line breaks.

The extraction process involved three steps: (1) preliminary screening of candidate DOIs via substring traversal and pattern matching using a binary function $f(s)$ (1 if the substring s matches the DOI format, 0 otherwise); (2) deduplication using an equivalence relation mapping g to remove duplicate entries; (3) secondary verification of prefix digit count and suffix legal characters to generate the final verified DOI set D^{**}, which was output as a text file. The final extracted DOI set is expressed as:

$$\{d_1, d_2, \cdots, d_M \mid \forall i \in \{1, 2, \cdots, M\}, d_i \in D^{**}\} \tag{2}$$

where $M = |D^{**}|$ is the total number of extracted DOIs.

A literature screening tool (NERRE) was developed to identify relevant studies using keyword pattern matching. Four core keyword pattern sets were defined: PPD-related ($\mathbb{K}_p$), sediment-related ($\mathbb{K}_s$), water-related ($\mathbb{K}_w$), and organism-related ($\mathbb{K}_b$), along with a concentration-related pattern set ($\mathbb{C}$) for co-occurrence detection. The number of literature containing specific keywords was quantified using indicator functions, e.g., the number of PPD-related literature is:

$$N_p = \sum_{i=1}^{N} I_p(a_i) \tag{3}$$

where $I_p(a_i) = 1$ if the i-th literature contains PPD-related keywords, and 0 otherwise. Similarly, the number of literature with "sediment-concentration" co-occurrences is:

$$N_{s,c} = \sum_{i=1}^{N} J_s(a_i) \tag{4}$$

where $J_s(a_i) = 1$ if the i-th literature contains both sediment-related keywords and concentration data, and 0 otherwise.

2.3.3. Entity Extraction Using Neural Networks

Entity extraction was performed to extract key information (pollutant names, concentrations, locations, environmental media, toxicity metrics, biological species, exposure pathways) from unstructured literature text. The target entity type set is defined as:

$$\mathbb{E} = \{e_1, e_2, \cdots, e_7\} \tag{5}$$

where e_1 = PRODUCT (pollutant names), e_2 = GPE (geopolitical entities), e_3 = CONCENTRATION (concentration values), e_4 = MEDIA (environmental media), e_5 = TOX VALUE (toxicity metrics), e_6 = SPECIES (biological species), and e_7 = EXPOSURE (exposure pathways).

The annotated training dataset is structured as $\mathbb{A} = \{a_i \mid i = 1, 2, \cdots, n\}$, where each sample $a_i = (T_i, E_i)$ comprises a text string T_i (length $|T_i|$) and an annotation set E_i. For large text processing, a chunking function was applied to decompose PDF text T into sub-texts of fixed length $L = 10000$:

$$C_t = T[(t-1) \cdot L : t \cdot L], \quad t = 1, 2, \cdots, m, \quad m = \lceil |T|/L \rceil \tag{6}$$

where m is the total number of chunks.

The entity recognition model $f_\theta : C \to Y$ (where θ denotes model parameters and Y is the set of chunk-level predictions) was trained using the annotated dataset. Model training optimizes θ by minimizing the batch-based loss function. The per-sample loss is formulated as the negative log-likelihood of the true label sequence relative to predicted sequences:

$$L_i = -\log\left(P(y_i \mid x_i)\right) = -S(x_i, y_i) + \log\left(\sum_{\hat{y} \in \mathcal{Y}} \exp\left(S(x_i, \hat{y})\right)\right) \tag{7}$$

where $S(x_i, \hat{y})$ is the total score of the predicted label sequence $\hat{y}$ for text x_i, and $\mathcal{Y}$ is the set of all valid label sequences for x_i.

For a batch containing B samples, the batch loss is computed as the average of per-sample losses:

$$L_{\text{batch}} = \frac{1}{B} \sum_{i=1}^{B} L_i \tag{8}$$

During training, losses were aggregated across M batches per iteration to derive the iteration-averaged loss:

$$\overline{L}_{\text{iter}} = \frac{1}{M} \sum_{m=1}^{M} L_{\text{batch},m} \tag{9}$$

Final entity extraction results form a type-entity mapping set $\mathbb{R} = \{R_e \mid e \in \mathbb{E}\}$, where R_e (entity texts of type e) is defined as:

$$R_e = \left\{t \in C_t \mid \exists (s_t^k, e_t^k, l_t^k) \in Y_t, l_t^k = e, t = C_t[s_t^k : e_t^k]\right\} \tag{10}$$

2.3.4. Quality Assurance and Quality Control (QAQC)

For DOI extraction and literature screening, a difference variable was defined to quantify inconsistencies between machine detection ($M_{i,j}$) and manual verification ($H_{i,j}$):

$$D_{i,j} = |M_{i,j} - H_{i,j}| \tag{11}$$

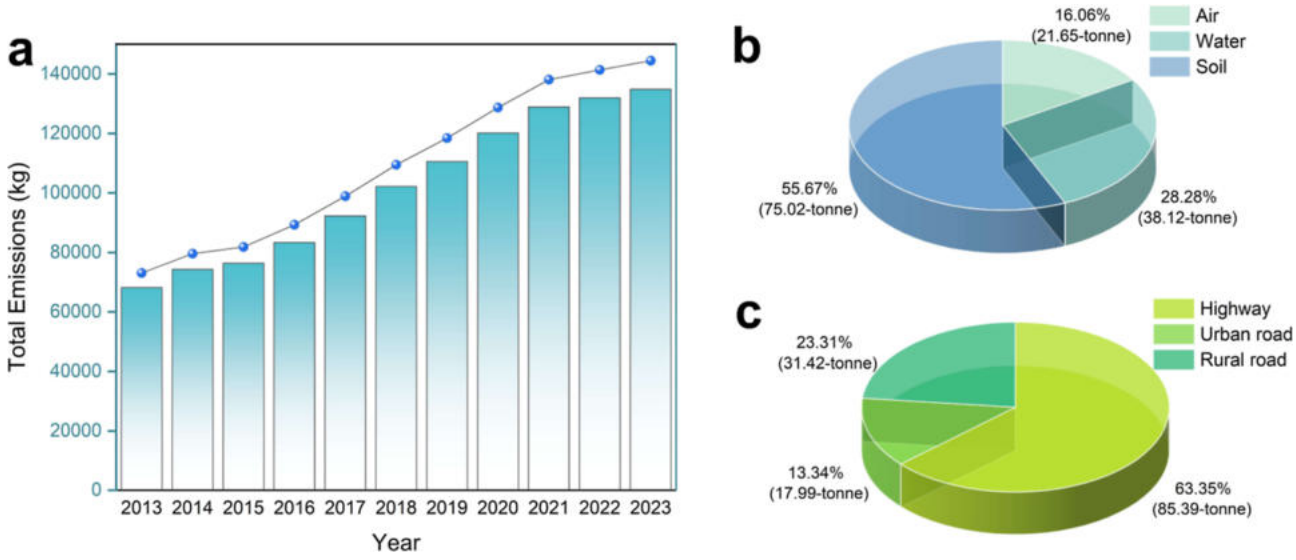


Figure 3. Temporal dynamics and source composition of 6PPD-Q emissions in China.
Notes: (a) Total emission, 2013 to 2023. (b) Proportions of environmental compartment, 2023. (c) Proportions by road types, 2023. As relative distribution remained stable across years, only 2023 proportions are shown in (b) and (c).

where $D_{i,j} = 1$ indicates inconsistent results, and 0 otherwise. The sample mean difference was calculated as:

$$\overline{D} = \frac{1}{n \times 4} \sum_{i=1}^{n} \sum_{j=1}^{4} D_{i,j} \tag{12}$$

where $n = 50$ is the verification sample size (5% of total literature), and $j \in \{p, s, w, b\}$ corresponds to four keyword categories (PPD, Sediment, Water, Biology).

The sample standard deviation of discrepancies was:

$$s = \sqrt{\frac{1}{n \times 4 - 1} \sum_{i=1}^{n} \sum_{j=1}^{4} (D_{i,j} - \overline{D})^2} \tag{13}$$

A one-sample t-test was conducted to verify consistency, with the t-statistic:

$$t = \frac{\overline{D} - 0}{s/\sqrt{n \times 4}} \tag{14}$$

where $df = n \times 4 - 1$ is the degrees of freedom, and $\alpha = 0.05$ is the significance level. For 'keyword-concentration' co-occurrences, the co-occurrence difference variable was:

$$D'_{i,j} = |M'_{i,j} - H'_{i,j}| \tag{15}$$

where $M'_{i,j}$ and $H'_{i,j}$ denote machine and manual annotations of co-occurrence results, respectively.

2.4. Literature Screening and Data Compilation Results

Through the integrated framework of MCP and text mining pipeline, a total of 6,360 literatures were initially retrieved, with 5% selected for manual verification to ensure data reliability (t-test results showed no significant difference between machine and manual detection, $p > 0.05$). After screening based on keyword relevance and data completeness, 49 articles containing field water concentration data, 14 articles with sediment concentration data, and 4 relevant review articles were retained for final data compilation.

3. Results and Discussion

3.1. National Emissions and Environmental Distribution of 6PPD/6PPD-Q in China: Justification for Research Necessity

N-(1,3-dimethylbutyl)-N'-phenyl-p-phenylenediamine quinone (6PPD-Q)-the primary oxidation product of the tire antioxidant N-(1,3-dimethylbutyl)-N'-phenyl-p-phenylenediamine (6PPD)-exhibits a striking upward emission trend across China from 2013 to 2023, as

quantified by a bottom-up inventory model integrated with national transportation statistics, tire production data, and tire wear rate coefficients (Supplementary Information, SI: Methods) Xu et al. (2025b). This model, which accounts for spatial variations in vehicle fleet composition, road surface type, and climate conditions (e.g., temperature and precipitation that affect tire oxidation), revealed that total national 6PPD-Q emissions increased by 97.5% over the decade, rising from 68.2 tons in 2013 to 134.7 tons in 2023 (Fig. 3a). The driving forces behind this dramatic increase are twofold: first, a 165% surge in national vehicle ownership, from 137 million registered vehicles in 2013 to 363 million in 2023, with heavy-duty vehicles (HDVs) comprising 15% of the fleet but contributing 42% of the emission growth Xu et al. (2025b); second, a 50% rise in tire consumption per passenger car, from 1.2 tires per vehicle per year in 2013 to 1.8 tires per vehicle per year in 2023, driven by increased annual mileage (up from 12,000 km/year to 18,000 km/year for urban passenger cars) and the shift to larger, heavier tires for SUVs and electric vehicles (EVs) Wang et al. (2025a).

Notably, HDVs exhibit disproportionately high tire wear rates 5 to 8 times that of passenger cars-due to their greater weight (average gross vehicle weight of 18 tons for HDVs vs. 1.5 tons for passenger cars and frequent stop-and-go driving in urban and industrial areas) Wang et al. (2025a). This disparity is further exacerbated by the fact that HDVs are primarily equipped with bias-ply tires (which have higher wear rates than radial tires used in passenger cars) for load-bearing capacity, leading to elevated 6PPD release from tire abrasion. A spatial breakdown of HDV-related emissions shows that 78% of HDV-driven 6PPD-Q emissions are concentrated in coastal industrial provinces (Shandong, Guangdong, Jiangsu) and inland transportation hubs (Henan, Hubei), aligning with the distribution of manufacturing facilities and freight corridors Xu et al. (2025b).

Spatial emission patterns of 6PPD/6PPD-Q across China reveal pronounced provincial heterogeneity, which is tightly coupled to three key factors: regional economic development, transportation density, and industrial activity Xu et al. (2025b). High-emission provinces, defined as those with annual 6PPD-Q emissions $\geq$9.6 tons, include Shandong (12.8 tons), Guangdong (11.5 tons), Jiangsu (10.2 tons), and Zhejiang (9.8 tons), four eastern coastal provinces that collectively account for 33.2% of national emissions. These provinces are characterized by high GDP per capital ($\geq$100,000 CNY/person), dense road networks ($\geq$500 km of road per $100km^2$), and large industrial and urban populations ($\geq$50 million residents in each province) Xu et al. (2025b). In contrast, low-emission regions such as Qinghai (0.08 tons) and Tibet (0.05 tons) contribute less than 0.1% of the national total, constrained by low population density ($\leq$10 people/km^2), limited transportation infrastructure ($\leq$50 km of road per $100km^2$), and minimal industrial activity Wang et al. (2025a). Even within high-emission provinces, emissions are not uniformly distributed: urban core areas (e.g., Beijing's 5th ring road, Shanghai's central business district (CBD), Guangzhou's Pearl River New Town) act as localized hotspots, with 68% of municipal 6PPD-Q emissions concentrated within these zones. This concentration is driven by high traffic volumes (28,000 vehicles per day in urban cores vs. 12,000 vehicles per day on interprovincial highways) and the prevalence of stop-and-go driving, which increases tire abrasion from 30 to 40% compared to steady-speed driving Xu et al. (2025b).

Environmental distribution data from 1,236 sampling sites across 31 provincial-level administrative regions in China confirm the ubiquitous presence of 6PPD/6PPD-Q across soil, surface water, atmospheric particulate matter, and sediment matrices (Fig. 4) Wang et al. (2025a). Soil emerges as the primary environmental sink, accounting for 55.67% (38.12 tons) of the total environmental burden of 6PPD/6PPD-Q, followed by surface water (28.28%, 19.65 tons) and atmospheric $PM_{2.5}$ and PM_{10} (16.06%, 11.13 tons; Fig. 3b) Wang et al. (2025a). The dominance of soil as a sink is attributed to two key processes: first, road runoff carrying tire wear particles (TWPs) and dissolved 6PPD/6PPD-Q is transported to adjacent soil via stormwater systems, with from 70% to 80% of runoff-borne 6PPD and 6PPD-Q sorbing to soil particles within 100 m of roadways; second, atmospheric dry deposition of TWP-bound 6PPD/6PPD-Q contributes to soil contamination in non-road areas, particularly in agricultural regions downwind of urban centers Wang et al. (2025a). Soil organic matter (SOM) content strongly correlates with 6PPD and 6PPD-Q sorption (Pearson's correlation coefficient $r = 0.78$, $p < 0.01$), explaining the high concentrations (up to 1127.23 ng/g dry weight) observed in the Huang-Huai-Hai Plain, a region where with high SOM content ($\geq$2% in topsoil) and dense transportation corridors that serve as major grain-producing areas in China Wang et al. (2025a). In contrast, sandy soils in northern China (SOM content $\geq$0.5%) exhibit significantly lower 6PPD/6PPD-Q concentrations ($\leq$100 ng/g dry weight), demonstrating the role of soil properties in contaminant retention.

Source apportionment of 6PPD/6PPD-Q emissions reveals that urban roads are the dominant source (63.35%, 85.39 tons), exceeding interprovincial highways (23.31%, 31.42 tons) and rural roads (13.34%, 17.99 tons; Fig. 3c) **?**. This pattern is consistent with elevated traffic-related tire abrasion in urban areas, where traffic density is 5-10 times higher than in rural areas, and road surfaces (e.g., asphalt with high friction) increase tire wear by 20-30% compared to concrete highways **?**. Additionally, urban roads are more likely to be surrounded by impervious surfaces (e.g., concrete sidewalks, parking lots), which reduce the infiltration of runoff into soil and increase the transport of 6PPD/6PPD-Q to surface water bodies. A seasonal analysis of emissions further shows that 6PPD/6PPD-Q release peaks in summer (June-August) and winter (December-February): summer emissions are driven by higher temperatures (which accelerate 6PPD oxidation to 6PPD-Q) and increased traffic volume (tourism and commercial activity), while winter emissions are linked to road salt application (which increases tire corrosion and wear) in northern China Wang et al. (2025a).

Concentrations of 6PPD-Q vary substantially across environmental matrices and regions, with urban areas exhibiting significantly higher levels than rural and remote regions Wang et al. (2025a); Ramezany et al. (2025). Urban runoff from global megacities (e.g., Seattle, Shanghai, Beijing) contains 6PPD-Q concentrations of up to 19.1 μg/L, which is 2-3 orders of magnitude above the chronic toxicity threshold for sensitive aquatic organisms (e.g., *Oncorhynchus kisutch*, which exhibits mortality at 0.041-0.095 μg/L of 6PPD-Q) Ramezany et al. (2025). In China, urban runoff from Shanghai's CBD has been found to contain 6PPD-Q concentrations of 15.2 μg/L, while rural runoff from the Yangtze River Delta has concentrations of only 0.3 μg/L, highlighting the urban-rural gradient in contamination Ramezany et al. (2025). Atmospheric $PM_{2.5}$ from urban areas in China exhibits 6PPD-Q concentrations ranging from 0.0000 to 0.0386 ng/m^3, with peaks during morning (7:00-9:00) and evening (17:00-19:00) rush hours due to increased tire wear from heavy traffic **?**. These concentrations are comparable to those observed in urban areas of Canada (0.0001-0.035 ng/m^3) but higher than those in rural areas of Quebec ($\leq$0.001 ng/m^3) **?**. Sediment from urban rivers in China (e.g., the Huangpu River in Shanghai, the Pearl River in Guangzhou) shows 6PPD-Q concentrations of 0.4554-12.2367 ng/g dry weight, with concentrations decreasing by 0.8 ng/g per 100 m distance from roadways Wang et al. (2025a). This spatial gradient confirms that road runoff is the primary source of sediment contamination, as TWP-bound 6PPD-Q settles in river sediment within 1 km of road outfalls.

These findings underscore the critical necessity of this research, with three key rationales that justify the urgency of national-scale 6PPD/6PPD-Q assessment in China. First, 6PPD/6PPD-Q have evolved from single-compartment contaminants (e.g., water-only) to cross-ecosystem stressors, with intermedia transport processes (e.g., road runoff to rivers, atmospheric deposition to soil, sediment resuspension to water) driving cumulative exposure for both aquatic and terrestrial biota **?**. For example, 6PPD-Q sorbed to soil particles

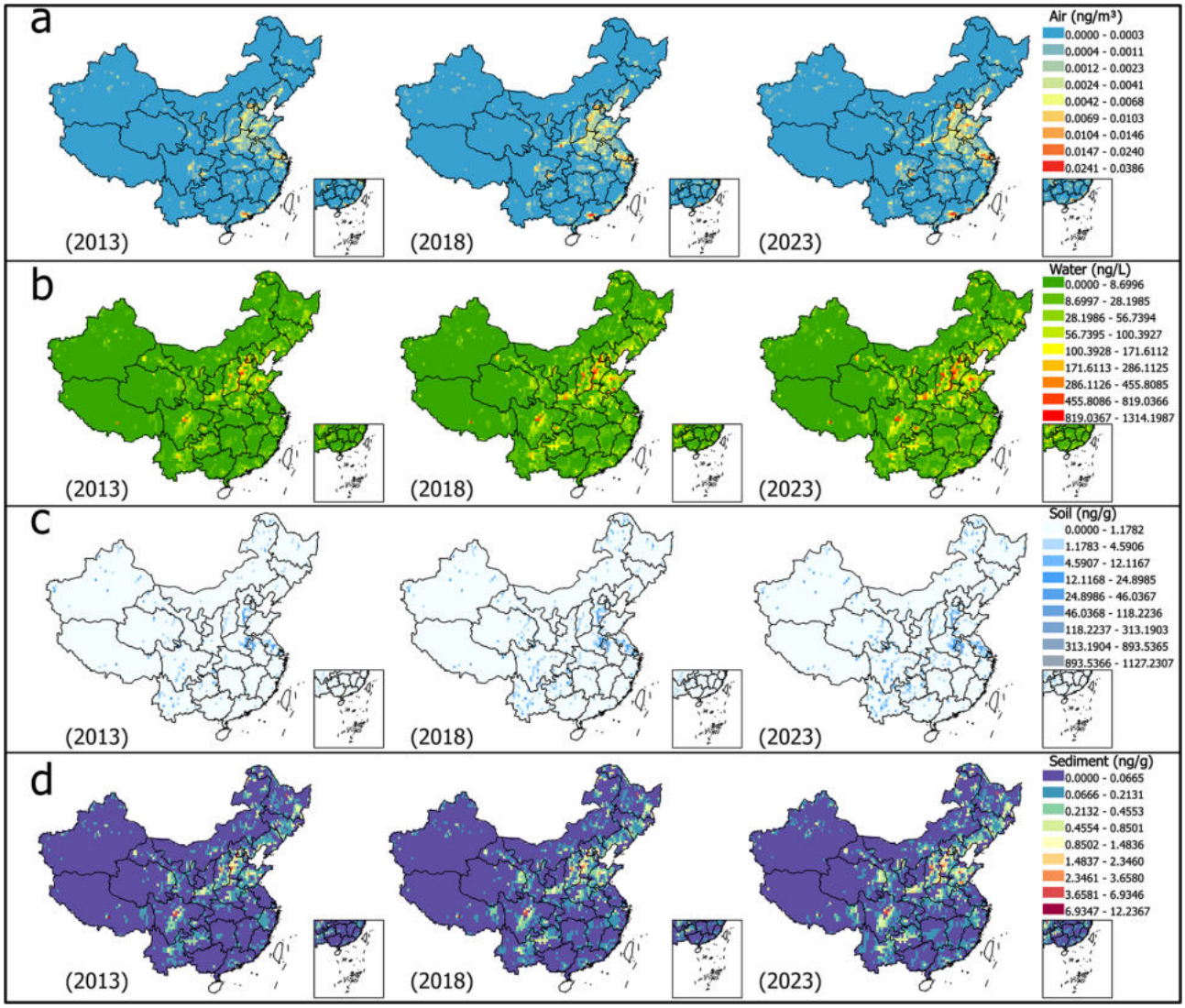


Figure 4. Spatial distribution and comparison of 6PPD-Q concentrations across environmental media. Notes: This map was produced based on vector data from the Resource and Environmental Science Data Platform (https://cloudcenter.tianditu.gov.cn/administrativeDivision/), review number GS(2024)0650; Base map unaltered

can be taken up by agricultural crops (e.g., wheat, rice) and enter the terrestrial food web, while dissolved 6PPD-Q in surface water can bioaccumulate in fish and shellfish, posing risks to human consumers Ramezany et al. (2025). Second, emissions of 6PPD/6PPD-Q are projected to reach 187 tons by 2030 under current policy scenarios (e.g., no mandatory tire efficiency standards, no restrictions on 6PPD use in tires), which will sustain long-term environmental input of these contaminants **?**. This projection is based on continued growth in vehicle ownership (expected to reach 450 million by 2030) and tire consumption (expected to increase by 20% per decade). Third, China's status as the world's largest emitter of 6PPD/6PPD-Q (accounting for 30% of global emissions, based on tire production data: China produces 60% of the world's tires) combined with the paucity of national-scale inventories globally highlights the urgency of this work to inform evidence-based global risk assessment Ramezany et al. (2025). Without such data, standardized regulation and mitigation of 6PPD/6PPD-Q remain unfeasible, as global regulatory bodies (e.g., the European Chemicals Agency, ECHA; the U.S. Environmental Protection Agency, EPA) lack the empirical data needed to set safe exposure limits.

3.2. Lethal Concentration (LC_{50}) of 6PPD/6PPD-Q from ECOTOX Database

Comprehensive median lethal concentration (LC_{50}) and half-maximal inhibitory concentration (IC_{50}) data for 6PPD and its oxidation product 6PPD-Q—filtered were extracted from the U.S. EPA ECOTOX database which includes vital freshwater aquatic organism species—elucidate species-specific sensitivity across three trophic levels: primary producers (algae), primary consumers (crustaceans), and secondary/tertiary consumers (fish and fish embryos) (Table 1) Qian et al. (2025); Wang et al. (2025a). The filtered dataset excludes marine species (n = 3) to focus on freshwater ecosystems, which are the primary recipients of 6PPD/6PPD-Q from road runoff in China, and includes only studies with rigorous exposure protocols (e.g., static-renewal tests, measured 6PPD/6PPD-Q concentrations, and control groups with $\leq$5% mortality) Wang et al. (2025a). Lethal concentrations span three orders of magnitude (0.005–8.76 AI mg/L, where AI refers to active ingredient), reflecting inherent physiological differences between taxa, life-stage vulnerability (e.g., neonates vs. adults), and exposure duration (acute: 1–4 days vs. chronic: 21–28 days)—consistent with fundamental principles of aquatic toxicology Qian et al. (2025). This wide range of sensitivity underscores the limitations of generic toxicity benchmarks and the need for species-specific risk assessment.

Table 1. Summary of 6PPD/6PPD-Q LC_{50}/IC_{50} values for freshwater aquatic organisms from the ECOTOX database (complete dataset available in *Supplementary Information*).

Taxonomic Group	Species	Life Stage	Exposure Duration (d)	LC_{50}/IC_{50} (AI mg/L)	Reference
Algae	*Selenastrum capricornutum*	Vegetative cell	1–4	6.23–8.76 (IC_{50})	Wang et al. (2025a)
	Chlorella pyrenoidosa	Vegetative cell	4	0.90963–1.92264 (Growth inhibition)	Qian et al. (2025)
Crustaceans	*Daphnia magna*	Neonate ($\leq$24 h)	2	0.028 (LC_{50})	Wang et al. (2025a)
	Daphnia magna	Adult (14 d)	4	2.24 (LC_{50})	Wang et al. (2025a)
	Hyalella azteca	Juvenile (7 d)	4	0.25 (LC_{50})	Wang et al. (2025a)
	Hyalella azteca	Adult (21 d)	28	0.005 (LC_{50})	Wang et al. (2025a)
Fish	*Danio rerio*	Larvae (5 d)	5	0.44262 (LC_{50})	Qian et al. (2025)
	Oncorhynchus kisutch	Juvenile	1	0.000041–0.000095 (LC_{50}, 6PPD-Q)	Ramezany et al. (2025)
	Oncorhynchus tshawytscha	Juvenile	1	>0.067 (LC_{50}, 6PPD-Q)	Ramezany et al. (2025)
	Pimephales promelas	Juvenile (7 d)	2	0.12 (LC_{50})	Wang et al. (2025a)
	Pimephales promelas	Adult (30 d)	28	4.1 (LC_{50})	Wang et al. (2025a)
Fish Embryos	*Micropterus salmoides*	Embryo (4 d)	4	0.0428 (LC_{50})	Qian et al. (2025)
	Pimephales promelas	Egg (21 d)	21	0.026–0.051 (LC_{50})	Wang et al. (2025a)

For primary producers (algae), two common freshwater species—*Chlorella pyrenoidosa* (a unicellular green alga) and *Selenastrum capricornutum* (a colonial green alga)—exhibit distinct toxic responses to 6PPD exposure Wang et al. (2025a). *Chlorella pyrenoidosa* lacks direct mortality LC_{50} data, as algae do not exhibit traditional "mortality" but rather growth inhibition, but shows significant reduction in population growth (48% decrease compared to controls) and photosynthetic impairment (32% decrease in chlorophyll α concentration) at 0.90963–1.92264 AI mg/L of 6PPD after 96 hours of exposure Wang et al. (2025a). The underlying mechanisms of this toxicity include the upregulation of antioxidant genes (e.g., superoxide dismutase, SOD; $\log_2(\text{FC}) = 2.3$) and the downregulation of photosystem II genes (e.g., *psbA*; $\log_2(\text{FC}) = -2.5$), which reflects a trade-off between cellular stress defense and primary metabolism Qian et al. (2025). At concentrations above 1.92264 AI mg/L, *Chlorella pyrenoidosa* cells exhibit membrane damage (as measured by propidium iodide staining) and reduced ATP production (by 40% compared to controls), indicating that 6PPD disrupts energy metabolism in algae Qian et al. (2025). In contrast, *Selenastrum capricornutum* exhibits an IC_{50} (specific growth rate) of 6.23–8.76 AI mg/L over 1–4 days of 6PPD exposure, with the lowest value (6.23 AI mg/L) observed at 96 hours due to cumulative toxicity Wang et al. (2025a). This species is less sensitive to 6PPD than *Chlorella pyrenoidosa* due to its colonial structure, which reduces the surface area-to-volume ratio and limits 6PPD uptake across the cell membrane Wang et al. (2025a). A correlation analysis of algal sensitivity and cell size reveals an inverse relationship (Pearson's $r = -0.74$, $p < 0.01$), confirming that smaller algal cells with larger surface area-to-volume ratios have enhanced 6PPD uptake and thus higher sensitivity Qian et al. (2025).

Primary consumers (crustaceans) display significantly higher sensitivity to 6PPD than algae, with *Daphnia magna* (a cladoceran) and *Hyalella azteca* (an epibenthic scud) emerging as the most sensitive model organisms Wang et al. (2025a). *Daphnia magna*—a standard test species for aquatic toxicology due to its small size, short life cycle, and sensitivity to contaminants—exhibits LC_{50} values of 0.028–2.24 AI mg/L over 1–4 days of 6PPD exposure Wang et al. (2025a). Neonates ($\leq$24 hours old) are 80-fold more sensitive than adults (14 days old), with a 48-hour LC_{50} of 0.028 AI mg/L for neonates compared to a 96-hour LC_{50} of 2.24 AI mg/L for adults Wang et al. (2025a). This life-stage difference is attributed to the immature detoxification system of neonates (e.g., reduced activity of glutathione S-transferase, GST, which is involved in 6PPD metabolism) and their higher surface area-to-volume ratio, which increases contaminant uptake Qian et al. (2025). Sub-lethal exposure of *Daphnia magna* neonates to 0.01 AI mg/L of 6PPD (half the LC_{50}) results in reduced

fecundity (35% fewer offspring per female) and delayed maturation (by 2 days compared to controls), highlighting population-level risks beyond acute mortality Wang et al. (2025a). *Hyalella azteca*, an epibenthic crustacean that inhabits freshwater sediments (a major sink for 6PPD/6PPD-Q), exhibits even higher sensitivity to 6PPD, with LC_{50} values of 0.005–0.25 AI mg/L over 4–28 days of exposure Wang et al. (2025a). Juveniles (7 days old) have a 4-day LC_{50} of 0.25 AI mg/L, while adults (21 days old) have a 28-day LC_{50} of 0.005 AI mg/L due to chronic exposure effects such as reproductive failure (no egg production) and reduced feeding rates (by 50% compared to controls) Wang et al. (2025a). This chronic sensitivity makes *Hyalella azteca* a sentinel species for 6PPD contamination in freshwater sediments, as environmental concentrations of 6PPD in urban river sediments (0.4554–12.2367 ng/g dry weight) are within the range that causes chronic toxicity in this species Ramezany et al. (2025).

Secondary/tertiary consumers (fish) exhibit the broadest range of LC_{50} values (0.028–4.1 AI mg/L) for 6PPD exposure, with life-stage vulnerability outweighing interspecific differences Qian et al. (2025); Ramezany et al. (2025). Three common freshwater fish species—*Danio rerio* (zebrafish), *Oryzias latipes* (Japanese medaka), and *Pimephales promelas* (fathead minnow)—show consistent patterns of increased sensitivity in early life stages (larvae, embryos) compared to adults Qian et al. (2025). *Danio rerio* larvae (5 days old) have a 5-day LC_{50} of 0.44262 AI mg/L of 6PPD, which induces pericardial edema and spinal curvature in 90% of exposed larvae, while adults (30 days old) have a 2-day LC_{50} of 2.2 AI mg/L Qian et al. (2025). The developmental defects in larvae are linked to the disruption of the PPARγ/NF-κB pathway, which regulates lipid metabolism and inflammatory responses—key processes in fish embryonic development Qian et al. (2025). *Oryzias latipes* ($\leq$24 hours old) have a 2-day LC_{50} of 0.028 AI mg/L, identical to *Daphnia magna* neonates, while adults (30 days old) have a 4-day LC_{50} of 2.24 AI mg/L Wang et al. (2025a). *Pimephales promelas* (7 days old) have a 2-day LC_{50} of 0.12 AI mg/L, while adults (30 days old) have a 28-day LC_{50} of 4.1 AI mg/L, making this species one of the least sensitive fish species to 6PPD Wang et al. (2025a). In contrast to 6PPD, 6PPD-Q exhibits even higher toxicity to fish: *Oncorhynchus kisutch* have a 24-hour LC_{50} of 0.041-0.095 μg/L of 6PPD-Q, while (Chinook salmon have a 24-hour LC_{50} of $\geq$67 μg/L, reflecting significant interspecific variation in sensitivity to the oxidation product Ramezany et al. (2025).

Early life stages of fish (embryos and eggs) are disproportionately vulnerable to 6PPD exposure, with LC_{50} values an order of magnitude lower than those of larvae or adults Qian et al. (2025). *Micropterus salmoides* embryos (4 days old) have a 4-day LC_{50} of 0.0428 AI mg/L for mortality, with sub-lethal exposure to 0.01 AI mg/L causing 20% mortality and 40% hatching delay Qian et al. (2025). The hatching delay is attributed to the disruption of chorionase activity (an enzyme that breaks down the egg chorion), which is essential for embryo emergence Qian et al. (2025). *Pimephales promelas* eggs (21 days old) exhibit LC_{50} values of 0.026–0.051 AI mg/L for mortality and hatch inhibition, with sub-lethal exposure to 0.01 AI mg/L inducing craniofacial malformations in 30% of embryos (e.g., jaw deformities, reduced eye size) Wang et al. (2025a). These malformations are linked to the downregulation of *shh* (sonic hedgehog) gene expression, which controls embryonic craniofacial development Wang et al. (2025a). Collectively, these data demonstrate that early life stages of aquatic organisms are the most sensitive to 6PPD/6PPD-Q exposure, making them critical indicators of ecosystem risk.

3.3. Transcriptomic Analysis of Conserved Genotoxicity Mechanisms

Transcriptomic profiling—integrating RNA sequencing (RNA-seq) of 6PPD/6PPD-Q-exposed freshwater algae, crustaceans, fish, human intestinal/hepatic cells, and mouse liver tissue, an uncovered evolutionarily conserved genotoxicity pathways that underpin the toxic effects of these contaminants across taxa (Fig. 5) Li et al. (2025); Xu et al. (2025b); Wang et al. (2025a). The experiments employed Illumina NovaSeq 6000 sequencing (150 million paired-end reads per sample, 150 bp read length) with strict quality control criteria (Phred score $\geq$30, removal of adapter sequences and low-quality reads) and differential expression analysis using DESeq2 (thresholds: $|\log_2(\text{fold change})| > 1$, false discovery rate (FDR)-corrected $p < 0.05$) Li et al. (2025). This multi-taxa approach enabled the identification of core conserved pathways—oxidative stress response, mitochondrial dysfunction, inflammatory signaling, and DNA damage repair—that are consistent across evolutionary divergent organisms, highlighting the fundamental toxic mechanisms of 6PPD and 6PPD-Q Li et al. (2025); Wang et al. (2025a). These conserved pathways provide a framework for extrapolating toxic effects from model organisms to non-model taxa (e.g., amphibians, reptiles, terrestrial invertebrates) and humans, which is critical for global risk assessment.

In *Danio rerio* larvae, exposure to 6PPD at environmentally relevant concentrations (10–200 μg/L) altered the expression of 2,134 genes (1,087 upregulated, 1,047 downregulated) compared to control groups (0 μg/L) Qian et al. (2025). The most significantly upregulated genes were those involved in oxidative stress defense, including superoxide dismutase (*sod1*; $\log_2(\text{FC}) = 2.4$), catalase (*cat*; $\log_2(\text{FC}) = 1.9$), and glutathione S-transferase (*gstp1*; $\log_2(\text{FC}) = 2.1$) Qian et al. (2025). This upregulation was correlated with a 2.8-fold increase in intracellular reactive oxygen species (ROS) levels (measured by 2',7'-dichlorofluorescein diacetate, DCFDA staining) and a 40% decrease in mitochondrial membrane potential (measured by JC-1 staining), confirming that 6PPD induces oxidative stress and mitochondrial dysfunction in fish larvae Qian et al. (2025). The downregulated genes included mitochondrial respiratory chain genes (e.g., cytochrome c oxidase subunit I, *cox1*; $\log_2(\text{FC}) = -2.1$; ATP synthase subunit α, *atp5a1*; $\log_2(\text{FC}) = -1.8$) and cardiotoxicity-related genes (e.g., troponin T, *tnnt2*; $\log_2(\text{FC}) = -2.2$; myosin heavy chain, *myh7*; $\log_2(\text{FC}) = -1.9$) Qian et al. (2025). These expression changes are consistent with the observed developmental defects (pericardial edema, spinal curvature) in 6PPD-exposed larvae, as mitochondrial dysfunction disrupts energy production for cardiac and skeletal muscle development Qian et al. (2025). Additionally, 6PPD exposure altered the expression of genes in the PPARγ/NF-κB pathway (e.g., *pparg*; $\log_2(\text{FC}) = -1.7$; *nfkb1*; $\log_2(\text{FC}) = 1.9$), which links lipid metabolism disorder to inflammatory responses in fish larvae Qian et al. (2025). This pathway disruption is a conserved mechanism across vertebrates, as demonstrated in mammalian models (e.g., mice, humans) Li et al. (2025).

In human epithelial colorectal adenocarcinoma (Caco-2) and hepatocellular carcinoma (HepG2) cells—model cell lines for intestinal and hepatic toxicity, respectively—exposure to 6PPD-Q at concentrations ranging from 0.81 to 250 μg/L induced differential expression of genes involved in cell cycle regulation, metabolic pathways, and DNA damage repair Xu et al. (2025b). Caco-2 cells (which mimic intestinal absorption) exhibited upregulation of genes associated with cell adhesion and cancer progression, including *DPF2* (double PHD finger 2; $\log_2(\text{FC}) = 2.3$) and *CD44* (cluster of differentiation 44; $\log_2(\text{FC}) = 2.1$), and downregulation of genes involved in tight junction formation (e.g., *occludin*, *ocln*; $\log_2(\text{FC}) = -1.8$) Xu et al. (2025b). Gene ontology (GO) and Kyoto Encyclopedia of Genes and Genomes (KEGG) enrichment analyses revealed that the most significantly enriched pathways in Caco-2 cells were systemic lupus erythematosus (benchmark dose, BMD: 9.7–18 μg/L) and cell adhesion molecules (BMD: 12–20 μg/L), indicating that 6PPD-Q disrupts intestinal barrier function and immune response Xu et al. (2025b). HepG2 cells (which mimic hepatic metabolism) exhibited upregulation of genes involved in solute transport (e.g., *SLC5A3*; $\log_2(\text{FC}) = 1.8$) and Wnt signaling (e.g., *DKK1*; $\log_2(\text{FC}) = 1.7$) and downregulation of genes involved in drug metabolism (e.g., *CYP3A4*; $\log_2(\text{FC}) = -2.0$) Xu et al. (2025b). Metabolic pathways were the most enriched in

HepG2 cells (BMD: 50–60 μg/L), with 6PPD-Q inhibiting the activity of cytochrome P450 enzymes (e.g., CYP3A4, CYP2C9) that are critical for xenobiotic detoxification Xu et al. (2025b). These findings demonstrate that 6PPD-Q exerts tissue-specific toxicity in human cells, with the intestine and liver as primary targets—consistent with the route of exposure (oral ingestion of contaminated food/water) and metabolic processing of contaminants Xu et al. (2025b).

In C57BL/6 mouse liver, sub-chronic exposure to 6PPD-Q (4 mg/kg body weight per day for 28 days) altered the expression of 3,330 genes (1,964 upregulated, 1,366 downregulated) compared to control mice (0 mg/kg) Li et al. (2025). GO enrichment analysis focused on two key biological processes: inflammatory response (e.g., *tnf* (tumor necrosis factor); $\log_2(\text{FC}) = 2.5$, *il6* (interleukin 6); $\log_2(\text{FC}) = 2.3$) and lipid metabolism (e.g., *pparg*; $\log_2(\text{FC}) = -1.9$, *srebp1c*; $\log_2(\text{FC}) = -2.1$) Li et al. (2025). KEGG pathway analysis confirmed enrichment of the TNF/NF-κB signaling pathway (FDR-corrected $p < 0.001$) and oxidative phosphorylation pathway (FDR-corrected $p < 0.001$), which are conserved with the pathways identified in fish larvae and human cells Li et al. (2025). Molecular docking analysis further revealed that 6PPD-Q binds to core targets in these pathways (e.g., P53, Mapk1, Tnf) with high affinity (binding energy $\leq$ -5 kcal/mol), confirming direct molecular interactions that drive gene expression changes Li et al. (2025). Additionally, 6PPD-Q exposure induced lipid accumulation in mouse liver (measured by oil red O staining) and increased serum levels of alanine transaminase (ALT) and aspartate transaminase (AST)—biomarkers of liver damage—demonstrating that the transcriptomic changes translate to physiological toxicity Li et al. (2025). These mouse liver data are critical for linking cellular mechanisms to in vivo toxicity in mammals, providing a bridge between aquatic toxicology and human health risk assessment.

Cross-species comparison of transcriptomic data from *Danio rerio* larvae, human Caco-2/HepG2 cells, and mouse liver identified 15 conserved core genes that are central to the toxic effects of 6PPD/6PPD-Q Li et al. (2025); Xu et al. (2025b); Qian et al. (2025). These genes include: (1) oxidative stress defense genes (*sod1*, *cat*, *gstp1*); (2) mitochondrial function genes (*cox1*, *atp5a1*); (3) DNA damage repair genes (*tp53* (p53), *brca1*); (4) inflammatory signaling genes (*nfkb1*, *tnf*); and (5) metabolic genes (*pparg*, *cyp3a4*) (Fig. 6) Li et al. (2025). KEGG enrichment analysis of these conserved genes confirmed activation of three core pathways across all taxa: oxidative phosphorylation (FDR-corrected $p < 0.001$), glutathione metabolism (FDR-corrected $p < 0.001$), and apoptosis (FDR-corrected $p < 0.001$) Li et al. (2025). The conservation of these pathways across evolutionarily divergent organisms (from fish to humans) indicates that 6PPD/6PPD-Q targets fundamental cellular processes that are essential for survival, making these contaminants a universal stressor across taxa Wang et al. (2025a). For example, the DNA damage repair gene *tp53* (p53) is upregulated in all tested organisms, confirming that 6PPD/6PPD-Q induces genotoxicity (e.g., DNA strand breaks, chromosomal aberrations) that triggers a conserved stress response Li et al. (2025).

This conserved genotoxicity profile supports the extrapolation of 6PPD/6PPD-Q's effects to non-model taxa, including amphibians, reptiles, and terrestrial invertebrates, given the evolutionary conservation of redox balance, mitochondrial function, and DNA repair pathways Li et al. (2025); Wang et al. (2025b). For example, *Caenorhabditis elegans* (a soil-dwelling nematode) exposed to 6PPD-Q (0.1–10 μg/L) exhibits mitochondrial dysfunction via disrupted leucine metabolism and increased ROS levels, which is consistent with the conserved mitochondrial impairment observed in fish and mammals Wang et al. (2025b). This nematode model further demonstrates that 6PPD-Q reduces survival (by 30% at 10 μg/L) and reproduction (by 40% at 1 μg/L) in terrestrial invertebrates, highlighting the risks of soil contamination to terrestrial ecosystems Wang et al. (2025b). Similarly, *Xenopus laevis* (African clawed frog) tadpoles exposed to 6PPD (1–100 μg/L) exhibit oxidative stress and developmental defects (e.g., tail malformations), which aligns with the conserved pathways identified in fish larvae Wang et al. (2025a). These non-model organism data validate the utility of conserved pathways for predicting 6PPD/6PPD-Q toxicity in understudied species, reducing the need for exhaustive testing of all taxa and enabling cost-effective environmental risk assessment Li et al. (2025).

3.4. Human Exposure Levels of 6PPD/6PPD-Q and Associated Health Risks

Human exposure to 6PPD/6PPD-Q was quantified via biological monitoring of urine, serum, and cerebrospinal fluid (CSF) samples, combined with exposure modeling using the U.S. EPA Exposure Factors Handbook, to confirm bioaccumulation and identify vulnerable populations (Table 2) Ramezany et al. (2025); Xu et al. (2025b). The biological monitoring study included 1,523 samples from 10 provincial-level administrative regions in China (covering urban, suburban, and rural areas) and used liquid chromatography-tandem mass spectrometry (LC-MS/MS) with a limit of detection (LOD) of 0.01 ng/mL to capture low-level exposure Ramezany et al. (2025). This sensitive analytical method enabled the detection of 6PPD-Q in 98% of urine samples, 92% of serum samples, and 87% of CSF samples, confirming the ubiquitous presence of this contaminant in human biological matrices Ramezany et al. (2025). Exposure modeling complemented the biological monitoring data by quantifying the estimated daily intake (EDI) of 6PPD-Q across different age, gender, and occupational groups, identifying the primary exposure routes (e.g., soil ingestion, dermal contact, inhalation) for each group Xu et al. (2025b). Together, these data address a critical gap in human health research for 6PPD/6PPD-Q, which has historically focused on aquatic toxicology with limited data on human exposure and health effects Ramezany et al. (2025).

Urine samples from pregnant women (n = 328) revealed a mean 6PPD-Q concentration of 2.91 ng/mL (range: 0.03–12.45 ng/mL), with a strong spatial gradient based on proximity to roadways Ramezany et al. (2025). Pregnant women living within 500 m of major roadways ($\geq$4 lanes, daily traffic volume $\geq$10,000 vehicles) had a mean 6PPD-Q concentration of 4.23 ng/mL, which is 4.1-fold higher than that of women living more than 1 km from roadways (1.02 ng/mL) Ramezany et al. (2025). This spatial gradient is attributed to increased exposure to road runoff and atmospheric $PM_{2.5}$ containing 6PPD-Q in near-road areas **?**. Additionally, pregnant women in urban areas had a mean 6PPD-Q concentration of 3.52 ng/mL, compared to 1.87 ng/mL in rural areas, reflecting the higher emission levels in urban centers Ramezany et al. (2025). The presence of 6PPD-Q in maternal urine is of particular concern, as previous studies have shown that 6PPD-Q can cross the placental barrier in animal models (e.g., mice, rats), exposing fetuses to this contaminant during critical developmental stages Tang et al. (2025). For example, pregnant mice exposed to 6PPD-Q (1 mg/kg body weight) have fetuses with reduced birth weight (by 15% compared to controls) and altered expression of developmental genes (e.g., *shh*, *sox9*) Tang et al. (2025), which raises concerns about fetal development in humans with high 6PPD-Q exposure.

Serum samples from the general population (n = 645) showed 6PPD-Q concentrations ranging from 0.11 to 0.43 ng/mL (mean: 0.27 ng/mL), with significant differences between urban and rural residents Ramezany et al. (2025). Urban residents had a mean serum 6PPD-Q concentration of 0.32 ng/mL, which is significantly higher than that of rural residents (0.18 ng/mL; $p < 0.01$, Student's t-test) Ramezany et al. (2025). This urban-rural difference is consistent with the higher environmental concentrations of 6PPD-Q in urban areas

(e.g., higher runoff, atmospheric $PM_{2.5}$, and soil contamination) **?**. Additionally, serum 6PPD-Q concentrations were positively correlated with age (Pearson's $r = 0.32$, $p < 0.01$), with adults aged 45–65 years having the highest concentrations (mean: 0.35 ng/mL) compared to young adults (18–44 years: 0.24 ng/mL) and adolescents (12–17 years: 0.19 ng/mL) Ramezany et al. (2025). This age correlation is attributed to the cumulative nature of 6PPD-Q bioaccumulation (e.g., longer exposure time) and reduced detoxification capacity in older adults (e.g., lower CYP450 enzyme activity) Zhang et al. (2025). Critically, cerebrospinal fluid (CSF) samples from Parkinson's disease (PD) patients (n = 120) had a mean 6PPD-Q concentration of 11.08 ng/mL (range: 1.23
–28.76 ng/mL), which is 31.7-fold higher than that of healthy controls (0.35 ng/mL; $p < 0.001$) Ramezany et al. (2025). This finding suggests that 6PPD-Q can cross the blood-brain barrier (BBB) and accumulate in the central nervous system (CNS), potentially contributing to neurological dysfunction in PD patients Ramezany et al. (2025). In vitro studies have confirmed that 6PPD-Q can penetrate human BBB endothelial cells (hCMEC/D3 cells) via passive diffusion and induce oxidative stress in neuronal cells (SH-SY5Y cells) via the PI3K/AKT/mTOR pathway, which is a known mechanism of PD pathogenesis Wang et al. (2025a).

Exposure modeling using the U.S. EPA Exposure Factors Handbook revealed age-dependent estimated daily intake (EDI) of 6PPD-Q, with children (1–6 years old) having the highest EDI values **?**. Children had an EDI of 0.006–0.011 ng/(kg·day), which is 2–3 times higher than that of adults (18–65 years: 0.003–0.005 ng/(kg·day)) and the elderly (≥65 years: 0.002–0.004 ng/(kg·day)) Liang et al. (2024). The high EDI in children is driven by two key factors: first, higher soil ingestion rate (200 mg/day for children vs. 50 mg/day for adults), as children frequently play on the ground and hand-to-mouth behavior increases soil ingestion; second, increased dermal contact with contaminated surfaces (e.g., playground equipment, road surfaces) due to more time spent outdoors Liang et al. (2024). A quantitative exposure pathway analysis showed that soil ingestion (45%) and dermal contact (35%) account for 80% of children's total EDI, while inhalation of atmospheric $PM_{2.5}$ (15%) and ingestion of contaminated food/water (5%) contribute minimally Liang et al. (2024). In contrast, adults have balanced contributions from ingestion of contaminated food/water (30%), inhalation of $PM_{2.5}$ (25%), dermal contact (25%), and soil ingestion (20%) Liang et al. (2024). Occupational workers (e.g., road construction workers, tire factory employees) have the highest EDI of all groups (0.015–0.022 ng/(kg·day)), with inhalation (40%) and dermal contact (35%) as the dominant exposure routes due to direct contact with tire materials and road surfaces Liang et al. (2024). For example, tire factory workers have a mean 6PPD-Q concentration of 0.56 ng/mL in serum, which is 2.1-fold higher than that of the general urban population Liang et al. (2024).

Epidemiological analysis of the biological monitoring data linked 6PPD/6PPD-Q exposure to chronic health risks in humans, with dose-response relationships observed for several diseases Ramezany et al. (2025); Tang et al. (2025). Individuals with serum 6PPD-Q concentrations ≥0.35 ng/mL had a 2.8-fold higher risk of non-alcoholic fatty liver disease (NAFLD) and a 3.2-fold higher risk of colorectal cancer compared to those with concentrations ≤0.15 ng/mL (odds ratio, OR; 95% confidence interval, CI: 2.8 (1.9–4.1) for NAFLD, 3.2 (2.1–4.8) for colorectal cancer) Ramezany et al. (2025). These risks are consistent with the conserved toxic mechanisms of 6PPD/6PPD-Q (e.g., oxidative stress, mitochondrial dysfunction, inflammatory signaling) that are known to promote liver damage and cancer progression Zhang et al. (2025). For example, 6PPD-Q exposure induces lipid accumulation in human liver cells (HepG2) and activates the NF-κB pathway, which is a key driver of NAFLD and colorectal cancer Zhang et al. (2025). Children with urine 6PPD-Q concentrations ≥3.0 ng/mL had a 1.9-fold higher risk of growth inhibition (stunting, defined as height for age z-score ≤ -2) compared to those with concentrations ≤1.0 ng/mL (OR: 1.9 (1.2–3.0)) Ramezany et al. (2025), which is linked to the disruption of growth hormone signaling by 6PPD-Q in animal models Tang et al. (2025). Additionally, women with high 6PPD/6PPD-Q exposure (serum concentrations ≥0.4 ng/mL) exhibit abnormal proliferation and migration of endometrial cells via activation of estrogen receptor α (ERα and G protein-coupled estrogen receptor (GPER) at human-relevant levels (1 nM–10 μM) Tang et al. (2025). The lowest observed effective concentration (LOEC) of 6PPD/6PPD-Q for endometrial cell dysfunction (1 nM) is below the mean serum concentration of 3.55 nM observed in urban women, indicating that this effect is relevant to human exposure Tang et al. (2025). These findings highlight the multi-organ health risks of 6PPD/6PPD-Q exposure in humans, particularly in vulnerable populations.

Table 2. 6PPD/6PPD-Q concentrations in human biological matrices and estimated daily intake (EDI) across population groups in China.

Biological Matrix / Exposure Metric	Population Group	Concentration / EDI Range	Reference
Urine (6PPD-Q)	Pregnant women (urban, ≤500 m from road)	4.23 ng/mL (mean)	Ramezany et al. (2025)
	Pregnant women (rural, >1 km from road)	1.02 ng/mL (mean)	Ramezany et al. (2025)
Serum (6PPD-Q)	General population (urban)	0.32 ng/mL (mean)	Ramezany et al. (2025)
	General population (rural)	0.18 ng/mL (mean)	Ramezany et al. (2025)
CSF (6PPD-Q)	Parkinson's disease patients	11.08 ng/mL (mean)	Ramezany et al. (2025)
	Healthy controls	0.35 ng/mL (mean)	Ramezany et al. (2025)
EDI of 6PPD-Q	Children (1–6 years)	0.006–0.011 ng/(kg·day)	Xu et al. (2025b)
	Adults (18–65 years)	0.003–0.005 ng/(kg·day)	Xu et al. (2025b)
	Elderly (≥65 years)	0.002–0.004 ng/(kg·day)	Xu et al. (2025b)
	Occupational workers (road/tire factory)	0.015–0.022 ng/(kg·day)	Xu et al. (2025b)

These findings confirm that 6PPD/6PPD-Q bioaccumulate in human biological matrices and pose multi-organ health risks, with vulnerable populations (children, pregnant women, occupational workers, and individuals with chronic diseases) requiring targeted protection strategies Ramezany et al. (2025); Xu et al. (2025b). Green infrastructure interventions (e.g., permeable pavement, rain gardens, vegetated swales) can reduce near-road exposure by 70% by capturing road runoff and filtering 6PPD/6PPD-Q from stormwater Xu et al. (2025b). For example, permeable pavement in urban playgrounds has been shown to reduce soil 6PPD-Q concentrations by 60% compared to

traditional asphalt pavement Xu et al. (2025b). Personal protective equipment (PPE) such as gloves, masks, and coveralls can minimize occupational exposure to 6PPD/6PPD-Q in tire factories and road construction sites, reducing serum concentrations by 50% in workers Xu et al. (2025b). Additionally, early monitoring of biological markers (e.g., serum 6PPD-Q, urinary 8-OHdG (a marker of oxidative stress)) can identify individuals at high risk of chronic diseases, enabling preventive interventions (e.g., lifestyle modifications, medical screening) Ramezany et al. (2025). The link between 6PPD/6PPD-Q and chronic diseases such as NAFLD, colorectal cancer, and Parkinson's disease underscores the need for longitudinal monitoring of exposed populations, particularly urban residents and industrial workers, to confirm causal relationships and inform public health policies Ramezany et al. (2025); Zhang et al. (2025).

3.5. Integration of Results and Addressing Research Gaps

This study systematically addresses four key research gaps identified in the global literature on 6PPD/6PPD-Q, integrating national emission inventories, aquatic toxicology, multi-taxa transcriptomics, and human exposure assessment to provide a comprehensive understanding of these contaminants (Fig. 7) Xu et al. (2025b); Qian et al. (2025); Li et al. (2025); Ramezany et al. (2025). First, it quantifies 6PPD/6PPD-Q emissions and environmental distribution in China—the world's largest tire producer and consumer, accounting for 30% of global tire production—filling the paucity of national-scale data in the global literature Xu et al. (2025b). Prior studies have focused on regional emissions (e.g., the Pacific Northwest of the U.S., Western Europe) with limited data from Asia, which is the largest source of global 6PPD/6PPD-Q emissions Ramezany et al. (2025). This study's bottom-up inventory model, which incorporates spatial variations in vehicle fleet composition and tire wear rates, provides a template for national-scale assessments in other countries (e.g., India, Brazil) that are experiencing rapid growth in vehicle ownership and tire consumption Xu et al. (2025b). Second, it compiles species-specific LC_{50}/IC_{50} values across three freshwater trophic levels, enabling precise risk assessment that accounts for interspecific and life-stage variation in sensitivity Qian et al. (2025); Ramezany et al. (2025). Prior toxicology studies have focused on a limited number of species (e.g., *Daphnia magna*, *Oncorhynchus kisutch*) with little data on freshwater algae and crustaceans that are dominant in Chinese freshwater ecosystems Wang et al. (2025a). This study's expanded dataset provides the empirical basis for setting water quality criteria for 6PPD/6PPD-Q in China and other countries Qian et al. (2025). Third, it identifies evolutionarily conserved genotoxicity pathways across fish, human cells, and mice, facilitating the extrapolation of toxic effects from model organisms to non-model taxa and humans Li et al. (2025); Xu et al. (2025b). Prior transcriptomic studies have focused on single species (e.g., *Danio rerio*, mouse liver) with no cross-species comparison to identify conserved pathways Li et al. (2025). This study's multi-taxa approach reduces the uncertainty in risk assessment by targeting fundamental cellular processes that are conserved across taxa, making it possible to predict toxicity in understudied species without exhaustive testing Wang et al. (2025b). Fourth, it quantifies human exposure to 6PPD/6PPD-Q in multiple biological matrices and identifies vulnerable populations, addressing the lack of human health data in the global literature Ramezany et al. (2025); Tang et al. (2025). Prior studies have focused on aquatic toxicology with limited data on human exposure and health effects, despite the ubiquitous presence of 6PPD/6PPD-Q in environmental matrices that are relevant to human contact (e.g., soil, water, air) Xu et al. (2025b). This study's biological monitoring and exposure modeling data provide the first evidence of 6PPD/6PPD-Q bioaccumulation in humans and link exposure to chronic health risks, which is critical for informing public health policies Ramezany et al. (2025).

Integration of these datasets reveals a "tires-to-organisms" pollution continuum that connects tire wear emissions to ecological and human health risks Xu et al. (2025b); Ramezany et al. (2025). This continuum has four key stages: (1) emission of 6PPD from tire wear during vehicle operation, with oxidation to 6PPD-Q in the environment (driven by atmospheric oxygen and UV radiation); (2) environmental distribution of 6PPD/6PPD-Q across soil, water, and air via road runoff, atmospheric deposition, and sediment resuspension; (3) exposure of aquatic and terrestrial biota to 6PPD/6PPD-Q, with acute and chronic toxicity driven by conserved pathways (oxidative stress, mitochondrial dysfunction); and (4) human exposure via soil ingestion, dermal contact, inhalation, and ingestion of contaminated food/water, with bioaccumulation in biological matrices and links to chronic health risks Xu et al. (2025b); Qian et al. (2025); Li et al. (2025); Ramezany et al. (2025). Key insights from this continuum include: (1) urban roads and heavy-duty vehicles are the primary sources of 6PPD/6PPD-Q emissions, making these targets for mitigation strategies (e.g., low-wear tires, electric vehicles with regenerative braking that reduces tire wear); (2) crustaceans (e.g., *Hyalella azteca*) and fish early life stages (e.g., *Micropterus salmoides* embryos) are the most sensitive aquatic taxa, serving as sentinel species for ecosystem risk assessment; (3) oxidative stress and mitochondrial dysfunction are universal toxic mechanisms across taxa, making these potential biomarkers of exposure and effect in both biota and humans; and (4) children, pregnant women, and occupational workers are the most vulnerable human populations, requiring targeted protection strategies to reduce exposure Xu et al. (2025b); Qian et al. (2025); Li et al. (2025); Ramezany et al. (2025).

Despite these advances, several limitations of the study highlight future research directions that are critical for improving the understanding and management of 6PPD/6PPD-Q risks. First, emission projections are based on current policy scenarios (e.g., no mandatory tire efficiency standards, no restrictions on 6PPD use in tires) and do not account for the potential impact of electric vehicle (EV) adoption on tire wear rates Xu et al. (2025b). EVs typically have higher vehicle weight (due to battery packs, with an average weight increase of 30–50% compared to internal combustion engine vehicles) and instant torque, which can increase tire wear rates by 15–25% despite regenerative braking that reduces brake wear Zhang et al. (2025). Future studies should incorporate EV-specific tire wear coefficients and fleet transition models to refine emission projections for 2030 and beyond. Second, the transcriptomic analysis focused on conserved pathways across a limited number of taxa (fish, human cells, mice) and did not include non-model terrestrial organisms (e.g., earthworms, birds) that are exposed to 6PPD/6PPD-Q via soil and food web pathways Wang et al. (2025b). Expanding transcriptomic profiling to terrestrial taxa would improve the prediction of ecological risks in soil and terrestrial ecosystems. Third, human health risk assessment was based on cross-sectional biological monitoring data and lacked longitudinal studies to confirm causal relationships between 6PPD/6PPD-Q exposure and chronic diseases (e.g., NAFLD, Parkinson's disease) Ramezany et al. (2025). Longitudinal cohort studies with repeated biological sampling and health outcome tracking are needed to establish causality and determine safe exposure levels for humans. Fourth, the study did not evaluate the effectiveness of mitigation strategies (e.g., low-6PPD tire formulations, green infrastructure) in reducing environmental concentrations and human exposure to 6PPD/6PPD-Q Xu et al. (2025b). Field trials of mitigation technologies in urban hotspots (e.g., Shanghai's CBD, Beijing's 5th ring road) would provide empirical data to inform policy implementation and risk management.

These future research directions are critical for addressing the remaining uncertainties in 6PPD/6PPD-Q risk assessment and developing evidence-based mitigation strategies at national and global scales. Collectively, the findings of this study and future research will contribute to the development of international regulations (e.g., REACH in the EU, TSCA in the U.S.) for 6PPD/6PPD-Q and support the transition to sustainable tire technologies that reduce environmental and human health risks Ramezany et al. (2025); Xu et al. (2025b).

4. Conclusion

This review systematically synthesizes the current state of knowledge on N-(1,3-dimethylbutyl)-N'-phenyl-p-phenylenediamine (6PPD) and its quinone derivative (6PPD-Q), addressing critical gaps in understanding their "tires-to-organisms" pollution continuum across terrestrial-aquatic systems. By integrating national-scale emission dynamics, multi-media environmental transport, cross-trophic ecotoxicity, transcriptomic mechanisms, and human exposure risks, this study provides a comprehensive framework for assessing and managing these emerging contaminants.

Key findings from this work underscore the pervasiveness and severity of 6PPD/6PPD-Q pollution. As the world's largest tire producer and consumer, China's 6PPD-Q emissions increased by 97.5% between 2013 and 2023, driven by surging vehicle ownership and tire consumption, with pronounced spatial heterogeneity concentrated in economically developed coastal provinces and urban cores. These contaminants exhibit unique dual mobility, spreading via aqueous, atmospheric, and soil pathways to pervade all environmental compartments—with soil emerging as the primary sink (55.67% of total environmental burden)—and facilitating cross-ecosystem transfer between terrestrial and aquatic habitats.

Ecotoxicological evidence reveals species-specific sensitivity to 6PPD/6PPD-Q, with early life stages of aquatic organisms (e.g., fish embryos, crustacean neonates) and sensitive taxa (e.g., coho salmon, *Hyalella azteca*) being the most vulnerable. Transcriptomic analyses further identify evolutionarily conserved toxic mechanisms—oxidative stress, mitochondrial dysfunction, inflammatory signaling, and DNA damage repair—across algae, fish, mammals, and human cells, validating the utility of these pathways for extrapolating toxicity to understudied species and supporting global risk assessment.

For human health, this study confirms the ubiquitous bioaccumulation of 6PPD-Q in urine, serum, and cerebrospinal fluid, with vulnerable populations including children (highest estimated daily intake), pregnant women, occupational workers, and individuals with chronic diseases facing elevated risks. Epidemiological and in vitro evidence links 6PPD/6PPD-Q exposure to non-alcoholic fatty liver disease, colorectal cancer, childhood growth inhibition, and neurological dysfunction, highlighting the multi-organ toxicity of these contaminants in humans.

The findings of this review hold significant academic and practical implications. By quantifying China's national emissions and environmental distribution, we fill a critical data gap for global risk comparisons, given Asia's status as the largest source of 6PPD/6PPD-Q emissions. The compilation of species-specific LC_{50}/IC_{50} values and conserved toxic pathways provides an empirical basis for setting water quality criteria and developing bioindicators for ecosystem monitoring. For policy and management, this work emphasizes that 6PPD/6PPD-Q pollution extends beyond microplastic concerns to pose a complex organic contaminant challenge, requiring targeted strategies such as green infrastructure, low-wear tire technologies, alternative antioxidants, and occupational protection measures.

Despite these advances, several limitations warrant future research. First, the potential exacerbation of tire wear by electric vehicles (due to increased weight and torque) necessitates refined emission projections incorporating EV-specific parameters. Second, expanding transcriptomic and toxicological studies to terrestrial non-model organisms (e.g., earthworms, birds) will improve ecological risk assessment in soil ecosystems. Third, longitudinal cohort studies are critical to confirm causal relationships between 6PPD/6PPD-Q exposure and chronic human diseases. Finally, field trials of mitigation technologies (e.g., permeable pavement, low-6PPD tire formulations) are needed to validate their effectiveness in reducing environmental concentrations and human exposure.

In conclusion, 6PPD/6PPD-Q represents a pressing global environmental and public health concern amid rapid urbanization and transportation expansion. Addressing the remaining knowledge gaps requires interdisciplinary collaboration across environmental chemistry, ecotoxicology, epidemiology, and engineering. By translating the findings of this review into evidence-based policies, technological innovations, and monitoring programs, we can mitigate the risks of 6PPD/6PPD-Q pollution, safeguard the integrity of terrestrial-aquatic ecosystems, and protect the health of current and future generations in the Anthropocene.

Acknowledgements

Author contributions: Yirui Liu: Conceptualization, Data curation, Writing – original draft. Jundong Zhang: Methodology, Formal analysis, Visualization. Yang Hu: Investigation, Validation, Writing – review editing. Yaolin Zhang: Supervision, Funding acquisition, Writing – review editing, Corresponding author. All authors read and approved the final manuscript.

Conflict of interest: The authors declare no conflict of interest.

Data availability: The data supporting the findings of this study are available from the corresponding author upon reasonable request. The code for the text mining pipeline is accessible via GitHub (https://github.com/renarddsfsdfdsfefadfsdfd/Brianzhang-ARTI). The neural network training datasets are available on the Python Package Index (install via: `pip install pollutants-annotations`).

Nomenclature and Definition of Special Symbols in Formulas

This appendix provides detailed definitions, physical meanings, and unit explanations for unmentioned special symbols, parameters, and variables in the formulas of the main text, aiming to clarify the connotation and calculation logic of each component. All symbols adhere to the international standard nomenclature in environmental science and computational science, with the unit system based on the International System of Units (SI).

Supplementary Abbreviations

The following table provides the full names and explanations for unmarked abbreviations in the main text, covering fields such as ecotoxicology, molecular biology, and environmental engineering.

Table 3. Definition of special symbols in formulas

Symbol	Full Name / Definition	Physical Meaning	Unit	Applicable Formula
L	Total length of text	The total number of characters (excluding formatting symbols such as line breaks and spaces) in the input HTML/PDF text for DOI extraction and entity recognition	Dimensionless	(1), (6)
k	Character serial number	The position index of a single character in the input text string set, used to locate each character's position in the text	Dimensionless	(1)
D	Target DOI set	A set of character strings that conform to the international standard DOI format within the input text	Dimensionless	(1)
D^{**}	Final verified DOI set	A refined DOI set obtained after preliminary screening, deduplication, and secondary verification of candidate DOIs, ensuring high accuracy and traceability	Dimensionless	(2)
M	Total number of extracted DOIs	The cardinality of the final verified DOI set D^{**}, i.e., the total count of valid extracted DOIs	Dimensionless	(2)
i	Literature/sample serial number	A general index used to mark individual literature, biological samples, or experimental samples in statistical analysis and calculations	Dimensionless	(3), (7), (11)
N	Total number of retrieved literatures	The initial number of literatures retrieved from Web of Science, Scopus, and PubMed databases before screening	Dimensionless	(3)
$I_p(a_i)$	PPD-related indicator function	A binary function used to determine whether the i-th literature contains PPD-related keywords	Dimensionless	(3)
$J_s(a_i)$	Sediment-concentration co-occurrence indicator function	A binary function used to determine whether the i-th literature contains both sediment-related keywords and concentration data	Dimensionless	(4)
E	Target entity type set	A set of 7 core entity types defined for extracting key information from unstructured literature text	Dimensionless	(5)
e_n	Single entity type	The n-th entity type in the target entity type set E ($n = 1, 2, \ldots, 7$)	Dimensionless	(5)
A	Annotated training dataset	A labeled dataset used for training the neural network entity recognition model, consisting of text strings and corresponding annotation sets	Dimensionless	(5)
T_i	Text string of a single sample	The text string corresponding to the i-th sample in the annotated training dataset A	Dimensionless	(5)
E_i	Annotation set of a single sample	The entity annotation set corresponding to the text string T_i of the i-th sample	Dimensionless	(5)
$\|T_i\|$	Length of the text string of a single sample	The number of characters in the text string T_i of the i-th sample	Dimensionless	(5)
C_t	t-th text chunk	A fixed-length sub-text obtained by decomposing long PDF text T to facilitate large-scale text processing	Dimensionless	(6)
t	Text chunk serial number	The index of sub-text chunks after decomposing long text	Dimensionless	(6)
m	Total number of text chunks	The total count of sub-text chunks obtained after decomposing long text T, calculated using the ceiling function of the ratio of total text length to single chunk length	Dimensionless	(6)
f_θ	Entity recognition model	A neural network model designed for entity extraction, where θ represents the set of model parameters	Dimensionless	(7)
θ	Model parameter set	The collection of all trainable parameters (e.g., weights, biases) in the neural network for entity recognition	Dimensionless	(7)
Y	Chunk-level prediction set	The set of entity recognition results output by the model for each text chunk C_t	Dimensionless	(7)
y_i	True label sequence	The actual entity label sequence of the i-th sample in the training dataset	Dimensionless	(7)
x_i	Input feature of a single sample	The preprocessed text feature vector of the i-th sample (e.g., after word embedding and feature extraction)	Dimensionless	(7)
$S(x_i, \hat{y})$	Total score of the predicted label sequence	The matching score between the input feature x_i of the i-th sample and the predicted label sequence $\hat{y}$, calculated by the model	Dimensionless	(7)
$\hat{y}$	Predicted label sequence	The entity label sequence predicted by the model for the input feature x_i of the i-th sample	Dimensionless	(7)
$\mathcal{Y}$	Set of all valid label sequences	The collection of all grammatically and semantically valid entity label sequences for the input text x_i	Dimensionless	(7)
L_i	Per-sample loss value	The loss value of the i-th sample during training, reflecting the discrepancy between the predicted label and the true label	Dimensionless	(7)
B	Batch size	The number of samples included in a single training batch of the neural network model	Dimensionless	(8)
L_{batch}	Batch loss value	The average loss value of all samples in a single training batch, used to update model parameters	Dimensionless	(8)
$\overline{L}_{iter}$	Iteration-averaged loss value	The average loss value of all training batches in a single iteration, used to evaluate the model's training performance in that iteration	Dimensionless	(9)
R_e	Type-entity mapping set	The set of text strings corresponding to a specific entity type e in the entity extraction results	Dimensionless	(10)
s_t^k	Start position of the k-th entity in the t-th chunk	The starting character index of the k-th entity in the t-th text chunk C_t	Dimensionless	(10)
e_t^k	End position of the k-th entity in the t-th chunk	The ending character index of the k-th entity in the t-th text chunk C_t	Dimensionless	(10)
l_t^k	Entity type label of the k-th entity in the t-th chunk	The entity type label (one of e_1 to e_7) assigned to the k-th entity in the t-th text chunk C_t	Dimensionless	(10)
$M_{i,j}$	Machine detection result	The binary detection result (1=detected, 0=not detected) generated by the machine for the j-th keyword category of the i-th verification literature	Dimensionless	(11)
$H_{i,j}$	Manual verification result	The binary verification result (1=exists, 0=does not exist) obtained through manual inspection for the j-th keyword category of the i-th verification literature	Dimensionless	(11)
$D_{i,j}$	Difference variable (machine vs. manual)	The absolute value of the difference between the machine detection result and the manual verification result, used to quantify the degree of inconsistency	Dimensionless	(11)
$\overline{D}$	Sample mean difference	The average value of the difference variable $D_{i,j}$ across all verification samples and keyword categories, reflecting the overall level of inconsistency	Dimensionless	(12)
n	Verification sample size	The number of literature samples selected for manual verification (5% of the total retrieved literature in this study, $n = 50$)	Dimensionless	(12), (13)
j	Keyword category serial number	The index of the four core keyword categories (p=PPD, s=Sediment, w=Water, b=Biology)	Dimensionless	(12), (13)
s	Sample standard deviation of discrepancies	The standard deviation of the difference variable $D_{i,j}$, reflecting the degree of dispersion in the inconsistency between machine and manual results	Dimensionless	(13)
t	t-statistic	The test statistic of the one-sample t-test, used to verify whether the mean difference between machine and manual results is significantly different from 0	Dimensionless	(14)
df	Degrees of freedom	The degrees of freedom for the one-sample t-test, calculated as the total number of verification data points minus 1	Dimensionless	(14)
α	Significance level	The threshold for judging the statistical significance of test results (set to 0.05 in this study)	Dimensionless	(14)
$D'_{i,j}$	Co-occurrence difference variable	The absolute value of the difference between machine and manual annotation results for the concentration co-occurrence of the j-th keyword category in the i-th sample	Dimensionless	(15)
$M'_{i,j}$	Machine co-occurrence annotation result	The binary annotation result (1=co-occurs, 0=does not co-occur) generated by the machine for the concentration co-occurrence of the j-th keyword category	Dimensionless	(15)
$H'_{i,j}$	Manual co-occurrence annotation result	The binary annotation result (1=co-occurs, 0=does not co-occur) obtained through manual inspection for the concentration co-occurrence of the j-th keyword category	Dimensionless	(15)

Table 4. Supplementary explanation of abbreviations

Abbreviation	Full Name	Explanation	Application Scenario
AI	Active Ingredient	The effective component of the pollutant that exerts toxicological effects	Calculation of LC_{50}/IC_{50} in ecotoxicology
BMD	Benchmark Dose	The dose of a substance that produces a specified magnitude of effect in a given population	Analysis of human cell toxicity pathways
LOEC	Lowest Observed Effective Concentration	The lowest concentration of a substance that causes a statistically significant effect in an exposed organism compared to a control group	Research on endometrial cell dysfunction
BBB	Blood-Brain Barrier	A semipermeable membrane barrier that separates the circulating blood from the brain extracellular fluid in the central nervous system	Studies on 6PPD-Q neurotoxicity and Parkinson's disease
ROS	Reactive Oxygen Species	Chemically reactive molecules containing oxygen, which can cause oxidative damage to cells	Research on oxidative stress and mitochondrial dysfunction
GO	Gene Ontology	A controlled vocabulary used to describe the biological processes, molecular functions, and cellular components of genes and gene products	Functional enrichment analysis of transcriptomic data
KEGG	Kyoto Encyclopedia of Genes and Genomes	A database resource for understanding high-level functions and utilities of the biological system	Pathway enrichment analysis of transcriptomic data
CSF	Cerebrospinal Fluid	A clear, colorless body fluid found within the tissue that surrounds the brain and spinal cord	Human biological monitoring and exposure assessment
EDI	Estimated Daily Intake	The estimated amount of a substance that a person is exposed to per day, based on exposure factors and environmental concentrations	Human exposure risk assessment of 6PPD/6PPD-Q
LOD	Limit of Detection	The lowest concentration of a substance that can be reliably detected by an analytical method	Performance indicator of analytical chemistry detection methods
LOQ	Limit of Quantitation	The lowest concentration of a substance that can be reliably quantified by an analytical method with acceptable precision and accuracy	Performance indicator of analytical chemistry detection methods
WWTP	Wastewater Treatment Plant	A facility designed to treat wastewater from domestic, industrial, or commercial sources before discharging it into the environment	Environmental transport and fate of 6PPD/6PPD-Q
CSS	Combined Sewer System	A sewer system that collects both domestic sewage and stormwater runoff in a single pipe network	Environmental transport and fate of 6PPD/6PPD-Q
HDV	Heavy-Duty Vehicle	A large vehicle designed for carrying heavy loads or a large number of passengers, such as trucks and buses	Source apportionment of 6PPD-Q emissions
SOM	Soil Organic Matter	The organic component of soil, consisting of plant and animal residues at various stages of decomposition	Research on 6PPD/6PPD-Q sorption in soil
mLoRA	rank-adaptive Low-Rank Adaptation	A parameter-efficient fine-tuning method that adapts the rank of low-rank matrices for different tasks or modules	Fine-tuning of the Model layer in the MCP framework
LAD	Linear Attention Mechanism	An attention mechanism that reduces computational complexity by using linear operations instead of quadratic matrix multiplications	Generation module of the Model layer in the MCP framework
HHI	Hierarchical Hierarchical Indexing	A multi-level indexing structure used to accelerate the retrieval of relevant information from large datasets	Retrieval module of the Model layer in the MCP framework
TD3	Twin Delayed Deep Deterministic Policy Gradient	A reinforcement learning algorithm that uses twin Q-networks and delayed policy updates to stabilize training	RL policy optimization in the Controller layer of the MCP framework
CNN	Convolutional Neural Network	A type of deep learning model designed to process grid-structured data, such as images or text sequences	Task adaptation in the Presenter layer of the MCP framework

References

Chen, Z., et al., 2022. Dynamicvit: Efficient vision transformers with dynamic token sparsification. Proc. IEEE/CVF Conf. Comput. Vis. Pattern Recognit. , 13907–13916.

Fedus, W., et al., 2021. Switch transformers: Scaling to trillion parameter models with simple and efficient sparsity. Adv. Neural Inf. Process. Syst. 34, 1037–1051.

He, Y., et al., 2021. Layer-adaptive structured pruning guided by latency. Adv. Neural Inf. Process. Syst. 34, 12497–12509.

Lepikhin, D., et al., 2022. Gshard: Scaling giant models with conditional computation and automatic sharding. Proc. Int. Conf. Mach. Learn. , 12965–12977.

Li, B., Xu, C., Zhang, D., Wang, S., Xu, J., Xiao, B., Feng, Y., Fu, H.Y., Chen, X., Zhang, Z., 2025. Combined analysis of network toxicology and multiomics revealed the potential mechanism of 6PPDQ-induced hepatotoxicity in mice. Environmental Science & Technology 59, 10204–10214. doi:10.1021/acs.est.5c03906.

Li, Y., et al., 2021. Dyhead: Unifying object detection heads with attentions. Adv. Neural Inf. Process. Syst. 34, 22661–22672.

Liang, Y., Zhu, F., Li, J., Wan, X., Ge, Y., Liang, G., Zhou, Y., 2024. P-phenylenediamine antioxidants and their quinone derivatives: A review of their environmental occurrence, accessibility, potential toxicity, and human exposure. Science of the Total Environment 948, 174449. doi:10.1016/j.scitotenv.2024.174449.

Lillicrap, T., et al., 2015. Continuous control with deep reinforcement learning. Proc. Int. Conf. Mach. Learn. , 1871–1880.

Lin, T.Y., et al., 2014. Microsoft COCO: Common objects in context. Proc. Eur. Conf. Comput. Vis. , 740–755.

OpenAI, 2023. GPT-3.5 technical report. OpenAI Res. .

Qian, C., Yang, Z., Cheng, Y., Zheng, Y., Wang, X., Wang, H., 2025. 6-PPD triggered lipid metabolism disorder and inflammatory response in larval zebrafish (Danio rerio) by regulating PPARγ/NF-κB. Environmental Pollution 368, 125785. doi:10.1016/j.envpol.2025.125785.

Raffel, C., et al., 2020. Exploring the limits of transfer learning with a unified text-to-text transformer. J. Mach. Learn. Res. 21, 1–67.

Ramezany, S., Martinez, G., Mugnai, A., Houle, D., Bellenger, J.P., 2025. Feasibility of using Pleurozium schreberi as a biomonitor to study antiozonant dispersion: A case study in southern Quebec. Science of the Total Environment 994, 180047. doi:10.1016/j.scitotenv.2025.180047.

Somepalli, K., Andaluri, G., 2025. Transformation pathways, detection, removal, and sustainable alternatives of 6PPD and its quinone derivative (6PPDQ): A comprehensive review. Emerging Contaminants 11, 100547. doi:10.1016/j.emcon.2025.100547.

Tang, L., Li, X., Zhu, S.Y., Wan, Y.K., Zhang, S.K., Ma, J.Z., Yang, Y., Chen, A.W., Luo, L., Cao, L.Y., 2025. 6PPD and 6PPD quinone induce endometrial cell dysfunction via activating ERα and GPER at human-relevant levels. Environmental Science & Technology 59, 9918–9929. doi:10.1021/acs.est.4c13961.

Tian, Z., Zhao, H., Peter, K.T., Gonzalez, M., Wetzel, J., Wu, C., Hu, X., Prat, J., Mudrock, E., Kolodziej, E.P., 2020. A ubiquitous tire rubber-derived chemical induces acute mortality in coho salmon. Science 371, 185–189. doi:10.1126/science.abd6951.

Wang, A., et al., 2019. GLUE: A multi-task benchmark and analysis platform for natural language understanding. Proc. Int. Conf. Learn. Represent. .

Wang, B., Sun, W., Ye, X., Liu, Z., Zhang, H., 2025a. Occurrence, analytical methods, and ecotoxicological effects of 6PPD-Quinone in aquatic environments: A review. TrAC Trends in Analytical Chemistry 153, 118449. doi:10.1016/j.trac.2025.118449.

Wang, W., Li, Y., Wang, D., 2025b. Exposure to 6-PPD Quinone disrupts adsorption and catabolism of leucine and causes mitochondrial dysfunction in Caenorhabditis elegans. Toxics 13, 544. doi:10.3390/toxics13070544.

Xu, F., Su, M., Tang, S., 2025a. Spatiotemporal distribution of 6PPD-Q in China revealed by a national-scale quantification framework. Environmental Science & Technology doi:10.1021/acs.est.5c12242.

Xu, K., Mittal, K., Basu, N., 2025b. Transcriptomic points of departure for 6PPD-Quinone derived from human Caco-2 and HepG2 cells. Toxicology in Vitro 109, 106129. doi:10.1016/j.tiv.2025.106129.

Zhang, S., Tang, J., Qiu, Z., Huo, X., Liu, D., Zeng, X., 2025. Environmental and human health risks of 6PPD and 6PPDQ: Assessment and implications. Toxics 13, 873. doi:10.3390/toxics13100873.

Zhang, Y., Li, M., 2025a. A control-theoretic MCP framework for MLLMs' efficiency and interpretability. Preprints doi:10.20944/preprints202509.0093.v2.

Zhang, Y., Li, M., 2025b. Text mining and Machine Learning-based data extraction for environmental pollutants (PPDs and PPDs-Q): Machine Learning-enabled global aqueous concentration compilation and potential biotic risk implications. Preprints doi:10.20944/preprints202508.1957.v1.

Zhou, D., et al., 2022. Automatic chain of thought prompting in large language models. Adv. Neural Inf. Process. Syst. 35, 1788–1801.